Louisiana Tech University

Louisiana Tech Digital Commons

Summer 8-2020

Lignin Ethanolysis Depolymerization and Product Upgrading with Mesoporous and Palladium Supported Zeolite Catalysts

Nathan Cody Baxter

LIGNIN ETHANOLYSIS DEPOLYMERIZATION AND PRODUCT

UPGRADING WITH MESOPOROUS AND PALLADIUM

SUPPORTED ZEOLITE CATALYSTS

by

Nathan Cody Baxter, B.S. M.S.

A Dissertation Presented in Partial Fulfillment
of the Requirements of the Degree
Doctor of Philosophy

COLLEGE OF ENGINEERING AND SCIENCE
LOUISIANA TECH UNIVERSITY

AUGUST 2020

LOUISIANA TECH UNIVERSITY

THE GRADUATE SCHOOL

JUNE 26, 2020

Date of dissertation defense

We hereby recommend that the dissertation prepared under our supervision by

Nathan Cody Baxter, B.S. M.S.

entitled **Lignin Ethanolysis Depolymerization and Product Upgrading with**

Mesoporous and Palladium Supported Zeolite Catalysts

be accepted in partial fulfillment of the requirements for the Degree of

Doctor of Philosophy in Engineering with a Micro & Nanoscale Systems Conc.

Shengnian Wang,
Supervisor of Dissertation Research

Shengnian Wang
Head of Engineering

Members of the Doctoral Committee:
Yuri Lvov
Joan Lynam
Heath Barnett
James Palmer

Approved:

Hisham Hegab
Dean of Engineering & Science

Approved:

Ramu Ramachandran
Dean of the Graduate School

GS Form 13a
(10/18)

ABSTRACT

Lignin is a high-volume farm waste and environmental hazard of paper and pulp industries. To promote the utilization of its rich aromatic units into important chemicals and fuels, efforts were intensively made to breakdown lignin structure with a variety of depolymerization processes involving heating, solvent, and catalysts or their combination. Among those processes, ethanolysis in supercritical conditions shows promising performance for its high lignin conversion and little char formation. To improve the yield and selectivity of aromatics, particularly phenols, we examined the important roles of acidity and pore structure of different zeolite catalyst play in this process. Zeolites with close micropores and acidity defined by their crystal structures including Beta, Y, and ZSM-5 were first examined. Zeolites with the same microporous structure but different acidic strength caused by various H-type sites were further evaluated. Comparisons were further made between HZSM-5 and HY zeolites with unique mesoporous structures and their counterparts with exclusive micropores. Despite the complexity of lignin depolymerization and its greatly diversified products, strong acidity was found effective to cleave both the C-O-C and C-C linkages on lignin structure to receive more phenols while mild acidity works mainly in ether bond breakdown. When the diffusion issues of gigantic lignin intermediate and monomer products are severe (e.g., in microporous zeolites), overall yield and selectivity of lignin depolymerization products fall and the pore size of catalyst becomes dominant between the two key factors. Like in many petrochemical reactions involving bulky molecules, hierarchical pore

structure also is important to promote mass transport and increase the exposure and utilization of acidic site inside zeolite catalysts. At the presence of mesopores in zeolites, their pore configuration is less sensitive when comparing with the acidity to decide the yield and selectivity to phenols of C_8-C_{11}. These findings provide important guidelines on the selection and design of zeolites with appropriate acidity and pore structure to facilitate lignin depolymerization or other cracking processes.

The products of lignin depolymerization are a mixture of various organic compounds including alcohols, ester, phenols, and other large hydrocarbons with high oxygen content (up to 40 wt.%), poor thermal stability, and low heating values (16-19 mJ/kg), insuitable to serve as alternative or replacement to fossil fuel. Hydrotreating step, a classic refinery process to remove oxygen and other unwanted elements in oil by adding hydrogen, is often suggested for the upgrading of bio-oil to increase its C/O ratio, improve its energy density, stability, as well as other required fuel properties. We successfully synthesized new mesoporous zeolites, Meso-ZSM-5, via solid-state crystallization of dry aluminosilicate nanogels. Palladium was further loaded on these zeolites to form a bi-functional catalyst (Pd/Meso-ZSM-5). When used in the hydrodeoxygenation of guaiacol, a major lignin depolymerization compound, Pd/Meso-ZSM-5 exhibits superior guaiacol conversion and product distribution when compared with those supported on conventional microporous ZSM-5 counterparts. This is attributed to the improved diffusion and accessibility of active sites inside Meso-ZSM-5 with its unique hierarchically porous structure formed through neighbor nanocrystals connecting at edges. Ring saturated hydrocarbons are largely produced at 200 °C when hydrogenation dominates while alkaylated aromatics become major HDO products as

deoxygenation becomes favorable at 250 °C. Unlike the disappointing conversion and severe coking issue over many HDO catalysts, this catalyst shows excellent anti-coking performance at various temperature conditions. These encouraging results demonstrated the great potential of Pd/Meso-ZSM-5 catalyst in bio-oil upgrading processes and may ignite the wide use in emerging renewable energy fields as well as many other reactions in traditional fossil fuel industrials.

APPROVAL FOR SCHOLARLY DISSEMINATION

The author grants to the Prescott Memorial Library of Louisiana Tech University the right to reproduce, by appropriate methods, upon request, any or all portions of this Dissertation. It is understood that "proper request" consists of the agreement, on the part of the requesting party, that said reproduction is for his personal use and that subsequent reproduction will not occur without written approval of the author of this Dissertation. Further, any portions of the Dissertation used in books, papers, and other works must be appropriately referenced to this Dissertation.

Finally, the author of this Dissertation reserves the right to publish freely, in the literature, at any time, any or all portions of this Dissertation.

Author _____

Date _____

DEDICATION

This dissertation is lovingly dedicated to my parents, Warner and Peggy Baxter.

Their support, encouragement, and constant love have sustained me throughout my life.

Thank you to my academic advisor, Dr. Shengnian Wang, who has guided me

throughout my graduate studies and in the process of finishing this dissertation.

TABLE OF CONTENTS

LIST OF FIGURES

LIST OF TABLES

ACKNOWLEDGMENTS

Firstly, I would like to express my sincere gratitude to my advisor Dr. Shengnian Wang for the continuous support of my Ph.D. study and related research, for his patience, motivation, and immense knowledge. His guidance helped me in all the time of research and writing of this dissertation. I could not have imagined having a better advisor and mentor for my Ph.D. study.

Besides my advisor, I would like to thank the rest of my advisory committee: Dr. James Palmer, Dr. Heath Barnett, Dr. Joan Lynam, and Dr. Yuri Lvov for their insightful comments and encouragement.

I am grateful to Mr. Davis Bailey and Ms. Debbie Wood for their generous help and support.

Special thanks is given to the other members in Dr. Wang's research group who assisted in this work, Dr. Yuxin Wang, Yixian Pei, Xuan Liu, Haixu Liao, and Sean Nations. Thank you for the time we spent together and the knowledge you have given me.

I would like to thank my family. My parents, Warner and Peggy Baxter, and my brother, Tim Baxter, who have given me their unending support through this entire endeavor.

CHAPTER 1

INTRODUCTION

1.1   Research Problems

1.1.1   Biomass, Bio-oil, and Bioenergy

As a future means of securing the energy supply, depolymerization of biomass has growing worth (Singh, S. *et al.*, 2014). It allows for reduction of fossil fuel emissions, provides a source of platform chemicals and supports the rural economy while reducing fossil fuel CO_2 emissions. First generation fuels and chemicals for this are high value sugars and oils. Second generation fuels and chemicals are in development, and are based on a cheaper source, lignocellulosic feedstock. The cell wall is composed of cellulose, hemicellulose, and lignin, with lignin being of primary importance. Lignin is amorphous, aromatic, and insoluble in water. It is a three-dimensional heterogeneous cross-linked polymer with low viscosity. It is very hard to isolate lignin from ligninocellulose due to its complex nature and must be modified to do so. Because lignin has reactions of carbon centered radicals leading to formation of new carbon-carbon linkages and thus char formation, it shows a refractory behavior towards conversion to low molecular weight compounds that can be used as starter chemicals and fuel additives.

1.1.2   Lignin Depolymerization

To separate lignin from the lignocellulosic biomass and further depolymerize it

into a useable form to produce different biofuels and bioproducts various methods have

been developed. Lignin depolymerization breaks down the complex aromatic structures

into simple compounds that can be used to make commercially important chemicals and

biofuels. Lignin depolymerization can be done by several chemical methods. Those are

thermal (e.g., pyrolysis, gasification), chemical (hydrogenolysis, ethanolysis, oxidation,

combustion) and thermochemical processes (combustion), depending upon what type of

lignin, which method uses depolymerization, and how efficient the degradation is for

particular products (Protasio, T. *et al.*, 2013). Hierarchically structured zeolites are

widely used in these depolymerization processes due to their unique solid acidity and

tunable pore structures.

1.1.3   Lignin Depolymerization Product Upgrading

The liquid bio oil from lignin depolymerization contains a significantly high

oxygen content (up to 40 wt.%) and upgrading is required prior to its use as high-valued

chemicals and fuels. Hydrodeoxygenation (HDO) serves as an efficient way to

simultaneously reduce the O/C ratio and increase the H/C ratio of bio oil to improve its

quality. HDO of bio-oil is done using two kinds of traditional hydrotreating catalysts, but

with either transition metal or precious metal loaded on solid acidic supports with

hierarchical porous structure. Product yields from these catalysts are either partially

hydrogenated oxygen-containing ones, e.g. phenol, catechol, cyclohexanol, or totally

hydrogenated compounds such as benzene and cyclohexane. Serious catalyst

deactivation arises because of the low stability of the lignin depolymerization product molecules.

1.2 Objectives and Approaches

In this dissertation project, we focus on investigating zeolites with appropriate acidity and unique pore structure to improve the lignin depolymerization in supercritical ethanol and its product from further upgrading with hydrodeoxygenation processes. Specifically, the following objectives and approaches are adopted:

1.2.1 <u>Investigate Roles of Acidity and Pore Structures of Zeolites on Lignin Depolymerization in Supercritical Ethanol</u>

We first examined the role that the solid acidity and pore structure of different zeolites play on lignin depolymerization in supercritical ethanol from the following aspects:

1. compare the lignin depolymerization performance on zeolites with similar micropore size (HZSM-5 and HBeta types) and similar solid acidity (HBeta and HY types),

2. compare the lignin depolymerization performance over zeolites with the same microporous structure but different acidic strength tailored by various ion-exchange levels,

3. compare the lignin depolymerization performance over HZSM-5 and HY zeolites with fin-like and worm-like mesoporous structures and their counterparts with exclusive micropores,

4. targeting effective cleavage of the C-O-C and C-C linkages on lignin structure and yield of phenol products.

1.2.2   Explore Hydrodeoxygenation of Bio-Oil Component with New Palladium

Catalyst Supported on ZSM-5 with Novel Mesoporous Structure (Pd/Meso-ZSM-5)

We then examined the hydrodeoxygenation of a classical lignin depolymerization

product component, guaiacol, over Pd/Meso-ZSM-5 from the following aspects:

1. how the new catalyst system contributes to guaiacol conversion and product

   distribution when compared with those supported on conventional

   microporous ZSM-5 counterparts,

2. how the new catalyst system contributes to improvement on diffusion and

   accessibility of active sites inside Meso-ZSM-5 with its unique hierarchically

   porous structure,

3. how the new catalyst system contributes to the improvement on anti-coking

   performance at various temperature conditions when compared with catalyst

   supported on conventional microporous ZSM-5 zeolites.

1.3   Dissertation Structure

Chapter 1 outlines the research problems and objectives of this research project. It

also introduces briefly the research approaches and organization of this dissertation.

Chapter 2 provides a literature review of relevant research work. This review includes the

overview of biomass, bioenergy, and bio-oil, various lignin depolymerization processes,

lignin depolymerization product upgrading through hydrodeoxygenation, and the current

state of one major catalyst and catalyst support—zeolites widely used in both lignin

depolymerization and depolymerization product upgrading processes. Chapter 3

investigates the important roles acidity and pore structure of different zeolites play in

lignin depolymerization in supercritical ethanol process. Chapter 4 demonstrates the great

potential of palladium/ZSM-5 with unique mesoporous structure catalyst in bio-oil upgrading. Chapter 5 summarizes the findings of the entire dissertation and recommends some work worthy of further exploration.

CHAPTER 2

LITERATURE REVIEW

2.1   Biomass as a Renewable Energy Source

Increased worldwide dependence on non-renewable fossil fuels and their

excessive use, particularly as transportation fuels, has caused serious consequences;

foremost are global warming and potential energy crises (Pang, S. *et al*., 2010). Overuse

has resulted in dwindling fossil fuel reserves, which may greatly impact our daily lives as

well as the energy supply security and economic development of many countries (Guo,

M. *et al*., 2015). Increased greenhouse gas emissions, chiefly carbon dioxide of which

two-thirds is caused by road transportation, is considered as directly responsible for

global warming (Guo, M. *et al.*, 2015; Pang, S. *et al*., 2010; Protasio, T *et al*., 2013).

These challenges have triggered the investment and involvement in the utilization of

renewable energy, which is nowadays the subject of multiple government policies (Guo,

M. *et al*., 2015). Among a variety of renewable energy forms, bioenergy and biofuel

alternatives seem attractive for multiple reasons. In terms of greenhouse gas emissions, it

can thus be said that that biomass is simply solar energy that has been captured. And,

increasing the use of this bioenergy is a prime opportunity to reduce emissions of fossil

fuels (Bernier, P. *et al*., 2013). In addition, for many countries, biomass is abundant and

the use of bioenergy accounts for a sizeable volume of renewable energy production

(Castillo-Villar, K. K. *et al.*, 2014).

Because of advantages, including no harmful emissions and abundant energy production, the use of bioenergy has drawn great attention from many countries in the past decade as an excellent source of alternative energy. In the EU, for example, reliance on fossil fuel has increased in the past few decades to the extent that nearly 84% of the transport fossil fuel is imported (Guo, M. *et al.*, 2015). In the United States, government policy directives require 100 billion liters of biofuel by the year 2022 (Roth, B. *et al.*, 2015). However, great challenges still exist on its massive and economical use. For examples, biomass is bulky with a low energy density, and issues with its seasonal supply are the primary obstacles precluding the use of biomass as a feasible energy source. Another hindrance is logistics costs. Besides the price, it is still debatable on the economic and environmental benefits bioenergy can bring to the world. We believe the answers are heavily dependent on which region is designated for its product, what kind of conversion technologies are available, and what products we receive eventually from this natural renewable energy format.

Plant biomass thus has been acknowledged as the most likely choice for fuels and energy (Pang, S. *et al.*, 2010). Investigations have been done on materials like forest residues including wood chips and sawdust as well as similar agricultural residues such as grass and crop waste (e.g., rice husks, coffee waste, sugar cane bagasse and bamboo cellulose pulp) (Pang, S. *et al.*, 2010; Protasio, T *et al.*, 2013). These forms of biomass are obtained from trees or crops that absorb carbon dioxide (CO_2) needed for photosynthesis so that they may grow. Large scale production of such biomass can not only increase profit of local businesses, but also potentially reduce the emissions of greenhouse gases, making the bioenergy production process become essentially a

supportable, renewable, and carbon dioxide neutral energy resource (Pang, S. *et al*., 2010). When properly managed, this allows not only replacement of fossil fuels (Roth, *et al*., 2015), but also benefits to the ecosystems of developing countries where the halting of deforestation, soil degradation, and enhancement of the carbon pool reduces greenhouse gas emissions considerably.

Assessment of sustainable bioenergy from forest products is fundamental in biofuel production and the search for alternative energy sources (Sacchelli, S. *et al.*, 2016). Biomass extraction can be done on multiple levels in an ecosystem and can be analyzed using multiple parameters. Wood and energy supply and demand can be based on regional levels, and should not be localized so that more diverse evaluations can be made. Territorial features should not be limited to only reduction of CO_2 emissions, but should encompass factors like forest fire risk reduction, estimation of biomass supply and demand, biomass quality, and local environment characteristics (Sacchelli, S. *et al.*, 2016).   Particularly, this is when reforestation and regeneration of crops is a factor (Zanchi, G. et al., 2012). Annual crops and felled forests cause a delay of many years to renew. This time period causes a delay between emissions of biofuels and their renewal or regrowth (Zanchi, G. et al., 2012).

All biomass has three major components, cellulose, hemicellulose, and lignin. Lignocellulosic component is the most abundant polymer on earth and is the waste of agriculture business, but is the product produced in pulp mills and used for paper and packaging business (Chen, J. *et al.,* 2016). Lignocellulosic biomass components are the primarily byproduct of these industries. Lignin's high density gives a high combustion yield and thus great heating values (Protasio, T. *et al.*, 2013). Fifty million tons of lignin

is estimated to be produced annually across the world, among which one third is burned

to produce waste heat and electricity in the paper mills themselves. Such large quantities

provide an almost unlimited supply for the manufacture of biofuels. Separating cellulose

in the lignin-hemicellulose matrix increases its degradation by enzymatic or other means

to convert each component into useable forms of chemicals and fuels that is imperative to

their full utilization. The lignin molecule structure consists of a guaiacly, syringyl, and p-

hydxoyphenly propane units in a three-dimensional configuration (Chen, J. *et al.,* 2016).

Traditionally, pyrolysis is used to convert the ligninocellulosic biomass into small

molecules containing aromatic ring structures. Desirable other functional groups

produced are phenolic hydroxyl, alcoholic hydroxyl, and meothxy and carboxyl groups.

These latter groups give lignin a highly reactive nature, and so the lignin is subjected to

further processing into renewable biofuels. Progress has been made on lignin

decomposition rates, the product yield and selectivity of its diverse products, and

potential applications of decomposition products (e.g., propanone and phenol

compounds) as gasoline and jet fuel in internal combustion engines without any need for

modification to those already existing engines.

2.2   Lignin Depolymerization

Due to its high energy content, lignin is used as a fuel energy source, with over

95% of all produced lignin has been for fuels and combustion (Wang, H. *et al.*, 2013).

Lignin depolymerization is intended to convert lignin from a complex compound into

small but high-valued aromatic chemical molecules to be used as fuels and other basic

chemicals, instead of simply burning for heating (Wang, H. *et al.*, 2013; ArneStahl, A. *et

al*., 2014). Some lignin types, particularly those containing sulphonates, can be made into

vanillin and similar products. Depolymerization of lignin is also useful for a variety of transportation fuels (Wang, H. *et al.*, 2013). Butanol and biodiesel are of particular importance (Welker, C. *et al.*, 2015). Such applications are shown considerable increase in use as petroleum prices escalate and demand for renewable energy increases (Wang, H. *et al.*, 2013).

As for lignin, it is comprised of polyaromatics with several basic phenol units (i.e., coumaryl, coniferyl, and sinapyl), which can become high-value aromatic feedstock and/or high-quality fuels. Pyrolysis (or other thermal processes) and solvent assisted processes have been introduced to help improve the cleavage efficiency of C-O-C and C-C linkages in its structure to release the rich phenol-type aromatics. There are three main classes of potential processes under consideration for depolymerization of lignin (Roth, B. *et al.*, 2015). They are high temperature thermal conversion, gasification, or pyrolysis that deliver light gaseous and condensable molecules that are subsequently transformed by established chemical processes. Renewable fuels can be similarly produced using pyrolysis and gasification. The products of these processes may further be transformed into aromatic compounds including benzene, toluene, xylene, and phenol through Fischer-Troph conversion of syngas, low temperature catalytic or enzymatic conversion that lead to high value products (Roth, B. *et al.*, 2015).

Most methods of depolymerization create poor products in low yields, but the depolymerization of oxidized lignin in acidic conditions can improve yields. Rahimi, et al. (ArneStahl, A. *et al.*, 2014) proposed a method that used aqueous formic acid to depolymerize oxidized lignin, primarily by C-O-C bond cleavage, with a more than 60% yield of low molecular weight aromatics (ArneStahl, A. *et al.*, 2014). But oxidation

causes some loss of carbon from lignin structure, making direct depolymerization a more favorable process in lignin utilization. However, lignin's complex structure makes it challenging to direct degrade completely. This has resulted in recent efforts in using catalysts to decompose the lignin. Catalysis have high activity, selectivity, and stability and so lend themselves well to use in lignin-to-chemicals conversion and the liquid products are then readily used in place of fossil fuels for energy sources and other valuable feedstocks (Chen, J. et al., 2016).

2.2.1   Thermal Depolymerization

When lignin undergoes pyrolysis, it is subjected to temperatures ranging from 300-1000 °C in the absence of air. Thermal decomposition of lignin results in three groups of products (Lou, R. *et al.*, 2010). They are the condensed liquid, the solid, and light gas. Because all plants vary in their chemical composition, this causes variations in the decomposed lignin product composition (Lou, R. *et al.*, 2010).   The solid is called the biochar and the light gas contains the CO, CO_2, CH_4, and other trace light hydrocarbon gases. The condensed liquid contains the hydrocarbons, aromatics, ketones, and phenolics as the bio-oil. Among all products, liquid bio-oils are the most abundant, generally comprising three-fourths of the total products of lignin thermal decomposition (Sukhbaatar, B. *et al.*, 2009).

Other useful organic products in bio oils include acids (Sukhbaatar, B. *et al.*, 2009; Nimmanwudipong, T. *et al.*, 2011). Acetic acid and formic acid are prime examples of water-soluble components useful for food products (Abdullah, N. *et al.*, 2013). These can be removed from the biofuels using ion-exchange resins made by produced phenol-formaldehyde resins. Lignin biomass is also a source of methyl tert-

butyl ether, ethyl tert-butyl ether, and tert-amyl methyl ether (Dautzenberg, G. *et al.*, 2011). These alkyl ethers improve combustion efficiency and enhance the octane number in gasoline. Biomass feedstocks are rich in heteroatoms, O and N, unlike typical petroleum-based feedstocks (Luque, R. 2014). Typical feedstocks are high in C and H. Removal of C and H require multiple steps to remove these molecules generating large heat losses. These difficulties in crude oil processing are insignificant when processing biomass to biofuels because the biomass feedstocks are in a comparable energy state as the products (Luque, R. 2014). Structurally, biomass contains cellulose and lignin (Mohammed, I., *et al*., 2015; Hughes, S. *et al*., 2014). Because lignin has a complex structure, it is difficult to separate it from lignocellulosic biomass for conversion to useful products without extensive alteration. These readily lend themselves to bio-oil production. Structural analysis shows that biomass has considerable cellulose and lignin contents which are good candidates for good quality bio-oil production. And, these have low levels of sulfur and nitrogen, and produce little char when thermally decomposed, making them quite environmentally sound (Mohammed, I., *et al*., 2015).

2.2.2   Solvent Assisted Depolymerization

Typical pyrolytic processes result in extensive formation of char due to reactions in which carbon centered radicals recombine and form new C-C linkages. Therefore, it is necessary to use other methods for conversion to biofuels. No practical methods exist for depolymerizing lignin using microorganisms or biological methods because lignin is not a good metabolic carbon or energy source (Chai, L. *et al.*, 2014). New investigation comprises using solvents as conversion agents, often in the presence of catalysts (Singh, S. *et al.*, 2014). Catalysts include water, acids, bases, methanol, ethanol, and ethylene

glycol. Choosing these compounds as catalysts also reduces the chance for repolymerization and char formation common in current pyrolytic decomposition methods and promote greater production of lignin to bio-fuels (Singh, S. *et al.*, 2014). Depolymerization can also be assisted with chemical agents. Depending on which chemical additive is used, lignin depolymerization can be categorized into five main areas: base-catalyzed, acid-catalyzed, metal-catalyzed, ionic liquid-assisted, and supercritical fluid-assisted (Wang, H. *et al.*, 2013). Repolymerization remains an issue, and other additives can be introduced in the depolymerization reaction vessel to prevent it (Diop, A. *et al*., 2015). Phenol can be added to suppress repolymerization and reduce char. This is useful when using methanol as the solvent and increases the amounts of phenolic products (Diop, A. *et al*., 2015). In many cases, the combination of solvent and catalysts is used to maximize the lignin conversion and product yield or selectivity.

2.2.2.1   Solvent Assisted Depolymerization

To mitigate the substantial char formation in pyrolysis depolymerization processes, in more recent years, solvent –based conversion methods have been used (Pang, S. *et al*., 2010). By using water and alcohols catalyzed by homogenous bases or acids, effective depolymerization with noteworthy reduction in char creation is possible (Pang, S. *et al*., 2010). Water can be used to provide a reaction medium for biomass conversion because it is the most plentiful, environmentally gentle solvent with exciting physiochemical properties at high temperature. Water at high temperatures is favorable for the removal of oxygen from biomass with an appropriate catalyst because it shows up to 3 folds of ionic product and an improved stability for small organic compounds and a lower dielectric constant. Using a common alcohol like methanol or ethanol or ethylene

glycol used as the solvent for lignin depolymerization has become a hopeful approach and is quite effective in avoiding repolymerzation of depolymerized lignin and consequent formation of char.

In many cases, solvents such as methanol serve as hydrogen donors in lignin conversion. To maximize the roles as hydrogen donor, water or other organic solvents in supercritical conditions were used for lignin depolymerization. For water, this is at temperatures ranging from 473K to 663K and pressure above 25 MPa. At supercritical conditions, water has a lower dielectric constant, weaker hydrogen bonds, and a high isothermal compressibility, making it especially useful for biomass decomposition reactions. If inorganic salts are involved, it is often preferable to have supercritical water as water with inorganic salts have relatively good solubility. But there are drawbacks to water in supercritical conditions, mainly coming from the harsh temperature and pressure conditions to reach supercritical conditions. This gives opportunities to other solvents such as alcohol or acetone whose supercritical conditions are relatively easier to accomplish. If operation conditions are suitable, there is high phenolic compound production and reduction of char formation as phenol acts as a capping agent (Bernier, P. *et al.,* 2013).

The lignin can be depolymerized, if under subcritical and supercritical conditions, >290 °C and 25-40 MPa, which produces aromatic monomers and gases. If Kraft or organosolv lignin is treated with soluble bases, KOH, NaOH, and CsOH, in CH_3OH or C_2H_5OH under supercritical conditions, chatechols and phenols are produced. Another method of yielding phenols and gases is to treat the lignin with supercritical water with p-cresol as the solvent. For the depolymerization of organosolv lignin, if a supercritical

CO_2/acetone/water fluid system is used at temperatures of 300-370 °C at 10 MPa pressure results in aromatic products, chiefly syringol and guaiacol. Even though all these methods can be used to depolymerize lignin, there are major disadvantages, particularly the high temperatures and high pressures. Because of the high temperatures there is also the risk of corrosion and loss of selectivity to aromatic monomers, which react further to produce gases, tar, and char.

2.2.3   Metal Supported Catalyst Depolymerization

In the presence of heterogeneous catalysts, such as metal supported catalysts including Pt, Ru, Pd, Ni, Co-Mo, and Ni-Mo on C, Al_2O_3, SiO_2, and combinations of the two latter and zeolites, depolymerziation reactions occur readily. When these are used, at temperatures of 150-300 °C lignin undergoes about 50% conversion and aromatic monomers and gases are formed. But there are drawbacks to this method, because using expensive H_2 is required and there is difficulty in catalyst recyclability due to sintering and leaching of the metals (Guo, M. *et al*., 2015).

In the case of metal supported catalysts, a study was done using a Ni-based catalyst for native birchwood lignin conversion (Guo, M. *et al*., 2015). This had a very high selectivity to monomeric phenols including propyl guaiacol and propyl syringol. More recently, a NiAu bimetallic catalyst was developed for the efficient hydrogenolysis of organosolv lignin into aromatic monomers under milder reaction conditions, e.g. low temperatures, in water. Also evaluated in hydrogenolysys of lignin C-O bonds into monomeric aromatic alcohols were NiRu, NiRh, and NiPd bimetallic catalysts at 100 °C and 0.1MPa pressure. Using a tungsten phosphide in hot compressed water-ethanol solvent at 280 °C and 2 MPa of H_2 resulted in production of phenols from alkaline lignin.

Kraft lignin can be converted into C_6-C_{10} esters, alcohols, arenes, phenols, and benzyl alcohols by using a process that utilized a nanostructured MoC catalyst at 280 °C in pure ethanol. For the hydrogenolysis and depolymerizatoin of organosolv lignin and the succeeding aromatic ring hydrogenation a single step method was studied using Cu-doped porous metal oxide in supercritical methanol at 300 °C. It has also been shown that lignin can be base-catalyzed depolymerized into aromatic monomers, or the BCD method. For this, at temperatures above 260 °C in the presence of nitrogen to obtain aromatic monomers, homogeneous bases can be used, including NaOH, KOH, and CsOH. The BCD method is not without its inadequacies. Harsh conditions, low selectivity toward desired aromatic product formation, necessity of a neutralization step, and corrosion of the reactor system are considerations. One alternative is to use a Ni-supported layered double hydroxide, or hydrotalcite. It could depolymerize the lignin without the use of external hydrogen and reduced metal (Guo, M. *et al*., 2015). To convert lignocellulosic solids into liquid fuels of C_2-C_6, or aliphatic alcohols, Cu-doped hydrotalcite based porous metal oxides in supercritical MeOH can be used (Guo, M. *et al*., 2015). Also, Lewis acids, particularly, $NiCl_2$ and $FeCl_3$, have been known to depolymerize alcell lignin into aromatic monomers. Catechols, guaiacols, and syringols are possible with this method. Using this, the highest conversions of lignin obtained were 30% from $NiCl_2$ and 26% from $FeCl_3$, both under reaction conditions of 305 °C and 1 hr reaction time.

2.2.4   Zeolites Involved Catalytic Depolymerization of Lignin

Zeolites with micropores (< 2 nm) or hierarchical porous structure that contains an additional meso- or macro-sized pore system) are of much interest in lignin depolymerization because they have high acidity and excellent thermal stability.

2.2.4.1   Microporous Zeolites

A zeolite is a microporous crystalline aluminosilicate, with many SiO_4 and AlO_4 tetrahedral structures held together by the corner linking oxygen atoms in certain regular manner (Rahman, M. *et al*., 2009; Bhardwaj, D. 2013). This gives zeolites a larger surface area and definite micropores with a pore size of 2 nm or less and a narrow size distribution (Rahman, M. *et al*., 2009). The Al3+ atom at the center of an AlO_4 tetrahedron contributes to the framework an overall negative charge that is neutralized by cations in zeolites. When these cations are removed by ion exchange, this gives a great number of acidic sites on the zeolite surface, which are believed to be the active sites in absorption of hydrocarbon molecules. Zeolites are therefore excellent mediators for adsorption and ion exchange. For the same reason, those acidic sites can absorb large hydrocarbon molecules and further crack into smaller molecules at the elevated temperature (Lutz, W. 2014). Since their introduction, zeolites are also widely used as cracking catalysts in fluid-cracking catalysts (FCC) and hydrocracking processes (Deng, Z. et al., 2015; Grigor'eva, N. et al., 2013).

2.2.4.2   Mesoporous Zeolites

In terms of pore diameters, macroporous zeolites, those with pores diameters greater than 50 nm, are more desirable than mesoporous zeolites, those with pore diameters of 2-20 nm (Garcia-Martinez *et al*., 2014; Roussel, T. *et al*., 2009).

Conventional zeolites, those that are completely microporous, do have unique properties, but are subject to too many constraints and limitations in reactions involving large molecules. Action, characterization, and lifespan in reactions of zeolites can all be enhanced by introducing ancillary mesoporostiy in the zeolite crystals. Not only do mesoporous zeolites have benefits in catalysis, but they also exhibit heightened performance in other routes including ion-exchange and adsorption (Perez-Remerez, J. *et al*., 2011). Recent years have seen amazing headway in the synthesis, categorization, and utilization of hierarchical zeolites with mesoporous structures (Perez-Remerez, J. *et al*., 2011; Wang, X. *et al*., 2010; Xiang, M. *et al.*, 2015).

Hierarchical zeolites are obtained by two principal routes (Ding, J. *et al.*, 2013). First is direct fabrication from large molecular templates like starch, carbon, resins, and surfactants. These templates are removed after crystallization via calcination. This method is costly, the synthetic procedures are intricate, the resulting products have poor mechanical properties, and atmospheric emissions from template combustion, particularly halogens, are severe. The second route is creation of mesopores in an already manufactured microporous zeolite. The mesopores are created with post-manufactured treatments in which either aluminum or silicon moieties are selectively detached from the zeolite structure. Resulting mesopore size can be difficult to control using these dealumination and desilication processes, and the severe conditions these processes involve can create flaws in the zeolites (Ding, J. *et al.*, 2013).

Post synthetic treatments, primarily dealumination and desilication, can change the zeolites by partial degradation of the zeolites so that they possess intra-crystalline mesopores necessary for large molecule catalysis (Deng, Z. *et al*., 2015). This has been

proven for zeolites by using dealumination with not just acids as traditionally done but even with silicates including ammonium hexafluorosilicate (Shin, H. *et al*., 2011). This involves an increase of the silicon to aluminum ratio within the zeolite framework (Shin, H. *et al*., 2011; Jo, C. *et al.*, 2014).

Dealmuination of zeolites is typically done using acids (Srivastava, R. *et al*., 2009). Particularly oxalic acid or tartaric acid are of choice for dealumination. Dealumination is performed on zeolite samples at different acid solution pH values under high temperatures or steaming at up to 500 °C. Zeolites treated with oxalic acid or tartaric acid at a pH of 2 or lower show highest activity. And, this activity increase at low pH can be interrelated with increase in accessibility of reactants to zeolite active site. Removal of aluminum in the framework causes this phenomenon. Dealumination is achieved by hydrolysis of Al-O-Si bonds combined with steaming (Srivastava, R. *et al*., 2009; Hosseini, M. *et al*., 2015). Aluminum forms a complex with the organic acids or it is directly replaced with silicon from gaseous silicon tetrachloride. Dealumination of an individual zeolite also is influenced by other factors including but not limited to acid site occurrence in the framework and defect sites within the framework of the zeolite crystal. Acid leaching with concentrated solutions of organic acids removes aluminum embedded in the structure of the zeolite from areas near defect sites and also from the outside surface of the zeolite. In the case of zeolite-γ, dealumination is very easy since there are many stacking defects already in its framework (Srivastava, R. *et al*., 2009; Jin, C. *et al*., 2010). Oxalic acid and citric acid dealumination of zeolite-γ is common, and aluminum species can actually be easily reintroduced in the structure by close control of the solution pH if so desired. If other mineral acids or other organic acids are used, there is greater

potential for loss of crystallinity and catalytic properties (Srivastava, R. *et al*., 2009; Hosseini, M. *et al*., 2015).   HZSM-5 stability is similarly affected by the same dealumination processes (Xu, B. *et al*., 2007; Zhang, H. *et al.*, 2013; Mitchell, S. *et al.*, 2012).

Recent attention has been directed towards modification of zeolites to obtain hierarchical porosity by desilication with alkaline media (Zhao, L. *et al.*, 2010). Investigation into different concentrations of alkali treatment to modify pore size and crystalline properties of ZSM-5 has been done. As alkaline concentration increases, so do total areas of the surface and mesopores, and volume and average pore diameter increase accordingly. Contrarily, micropore volume and surface area decrease and the samples become much more amorphous (Zhao, L. *et al.*, 2010). The effectiveness of desilication is influenced by aluminum content, changes in NaOH concentration, treatment time, and temperature. Manipulation of these factors allows control over resulting mesopore diameter and volume. If performed at optimum conditions, it does not necessarily eliminate micropores or reduce mesoporosity, and structural integrity is not lost. There is some loss of micropore volume, but this is owed to amorphous species inside the microchannels. Washing with dilute acid solutions can restore Micropore volume loss (Martinez, C. *et al*., 2014).   Attention has also been brought to cation exchange in zeolites (Zhen, S. *et al*., 2000). Properties of zeolites including thermal stability, adsorption characteristics, and catalytic nature are all dependent on what types and abundance of exchangeable cations within available sites on the catalyst (Zhen, S. *et al*., 2000).

Nanocasting with a hard template, when considering traditional template and non-template methods, is very desirable because the porosity of the synthesized materials, if control of the original template properties is done, can be easily and specifically designed. These hard templates include various carbon types, aerogels, and other porous materials (Castillo-Villar, K. *et al.*, 2014).

Soft templates including n-butylamine (BTA), ethylamine (ETA), isopropylamine (IPA), tetrapropylamine bromide (TPAB), ethylenediamine (EDA), ethanol (ETL), ethanol–ammonium (ETL–AM) have been used to successful synthesis of zeolites in hydrothermal environments (Sang, S. *et al.*, 2004). Template selection, gel composition, reagent properties all influence the final zeolites physical and chemical properties. So, template selection is vital for robust zeolite synthesis. If no template is used, structural solidity of the synthesized ZSM-5 will be too low. For zeolites synthesized without a template and SiO_2/AlO_2 ratios greater than 50, quartz appears and so the number of acid sites is lowered dramatically (Sang, S. *et al.*, 2004).

2.2.4.3   Zeolites in Lignin Depolymerization

The high silicate content allows zeolites to readily absorb water, in turn serving well as proton conductors (Baglio, V. *et al.*, 2005). The great number of Bronstedt acidic sites on the surface of zeolites allow hydrocarbon molecules absorption and further cracking into smaller compounds at the elevated temperature (Lutz, W. 2014). Therefore, zeolites are wide used as cracking catalysts in fluid-cracking catalysts (FCC) and hydrocracking processes since their introduction (Deng, Z. *et al*., 2015; Grigor'eva, N. *et al*., 2013). In the refining industry, zeolites have continually become more irreplaceable as catalysts. Production was about 625×10^6 tons in 2004 and is ever increasing. FCC

currently ranks second in the industry of all heterogeneous catalyzed processes in which

Zeolite H-Y is the active catalyst. As FCC process utilizes high molecular weight feeds,

so similar interest is thought effective in lignin molecule cracking within zeolite pores

(Garcia-Martinez, J. *et al*., 2014). A few reports exist of solid acid such as zeolites

assisted depolymerization of lignin.

These are typically done at temperatures higher than 340 °C to obtain aromatics

and gases. One instance is that where H-ZSM-5 zeolite was used at 340-410 °C in a

fixed-bed microreactor. This was used to upgrade pyrolysis oil to return C_5-C_{10}

hydrocarbons. Overall, the distillate hydrocarbons were 83 wt.% and the maximum

organic distillate obtained from upgrading the entire bio-oil was 19 wt.% of bio-oil.

Further examination at 700 °C for pyrolysis of kraft lignin in the presence of $NiCl_2$ and

H-ZSM-5 zeolite. In the catalytic fast pyrolysis of alkaline lignin into aromatics and

gases, properties of acidity and pore size variation have been presented. Studies have

shown that when cleaving ether bonds in lignin and improving its decomposition of

aliphatic hydroxyl, carboxyl, and methoxy groups that zeolites are helpful. Such zeolites

as MFI (Z), FAU (Y), BEA (B), FER (F), and MOR (M) zeolites when pyrolized with

softwood Kraft lignin that a one-step thermal conversion of lignin yields gasoline-range

liquid products. H-USY zeolite has proven useful with the process of pyrolysis of

alkaline lignin at high temperatures. Pyrolysis has predominantly been used in previous

studies of the depolymerization of lignin involving acid catalysts, and, in most of the

reactions, high temperatures are engaged. Such high temperatures always show the

formation of char and coke and includes the formation of gases. So, a low return of

aromatic monomeric products is obtained. Usually model compounds have been used in

these experiments such as dimers and trimers, thus it turns out to be very hard to replicate any results obtained in these reactions with the actual substrates. This is because they have highly complicated structures and impurities in comparison to model compounds (Guo, M. *et al.*, 2015).

As the catalyst supports, zeolites are also better suited than are amorphous oxide supports because they contain a higher amount of medium acid sites (Hanaoka, T. *et al.*, 2015). Zeolites with a high silica content gives immense practical value to the transformation of raw hydrocarbons to gasoline and fuels (Velichkina, L. *et al.,* 2009). The sole renewable energy source for conversion to jet fuel is biomass, and since fuel consumption efficiency is much higher in planes and air transportation, liquid hydrocarbons as fuels have great promise in air transportation applications (Hanaoka, T. et al., 2015). New technology and investigation of new catalysts creates a pathway to the reduction of aromatic and olefin content in fuels without lowering octane number (Velichkina, L. *et al.,* 2009).

2.3   Bio-oil Upgrading with Catalytical Hydrodeoxygenation

The liquid bio oil received from biomass decomposition contains a significant water fraction of 10-30 weight percent and also present are aldehydes, acids, carbohydrates, phenolics, ketones, alcohols, and a host of other products. It is unsuitable for transport fuel for several reasons. The presence of aldehydes, acids, and phenols in bio-oil give it detrimental properties including high viscosity, low heating value, and corrosiveness (Zhou, M. et al., 2017). Its high oxygen (up to 40 wt.%) and low hydrogen content also make bio-oil have low thermal/chemical stability and low calorific value. All these factors rendering the direct use of bio-oils as transport fuel inappropriate.

Upgrading processes such as catalytic hydrodeoxygenation (HDO) is used to reduce the

O/C ratio and increase the H/C ratio of bio-oils. Most oxygen in bio-oil presents as -OH

groups, C=O groups, and -OCH$_3$ groups. Unlike other upgrading processes that the

oxygen associated carbon will lose with the removal of oxygen, HDO under hydrogen

pressure has major byproducts of only H$_2$O and CH$_3$OH (Lu, M. *et al.*, 2016). Therefore,

bio-oils that are upgraded by hydrodeoxygenation can retain most carbon in the alkane

bio-oil with high H/C ratio (Wang, L. et al., 2015).

2.3.1   <u>Hydrodeoxygenation of Bio Oil using Sulfurized CoMo and NiMo Catalysts</u>

Catalytic hydrodeoxygenation is done using two kinds of catalysts, similar to

what are used in conventional hydrotreating refining catalysts (Lu, M. *et al*., 2016).

Sulfurized CoMo and NiMo catalysts, the most common superior hydrodesulfurization

and hydrodenitrogenation catalysts, were also used in catalytic HDO of bio-oil. Two

major disadvantages exist in their use for bio-oil upgrading: (1) Bio oil has a low sulfur

content and the use of sulfide catalyst introduces sulfur in its upgrading product to

contaminate the upgrading product; (2) the catalysts have an unstable sulfide structure

and sulfur must be uninterruptedly added to keep the catalysts sulfurized state. An

additional desulfurization process must be added after bio-oil upgrading. Product yields

from these sulfurized catalysts are either partially hydrogenated oxygen-containing ones,

e.g. phenol, catechol, cyclohexanol, or totally hydrogenated compounds such as benzene

and cyclohexane (Zhou, M. *et al.*, 2017). These products can easily be blended with

petroleum fuel in transport fuel applications. Cyclohexane, toluene, and xylene have

suitable vapor pressure and carbon number that facilitates their use in gasoline. Catalyst

in HDO reaction are quickly deactivated because of the low stability of intermediate aromatic molecule.

For non-noble metal catalysts, Ni and Fe are good candidates for phenol conversion. Recent studies of monometallic Ni-based catalysts with HDO reaction are done at temperatures greater than 300 °C and hydrogen pressures above 8 MPa. These are harsh conditions. Adding Co to the Ni as an active metal for ring opening through HDO of GUA could increase deoxygenation activity. In short, it is necessary that for hydrodeoxygenation of phenols and bio oil, Ni-based catalysts must be modified for higher activity at conditions of low pressures and temperatures (Zhou, M. *et al.*, 2017). Under high hydrogen pressure, complete conversion of bio-oil compounds is possible with relatively low temperatures (e.g., 250-350 °C) (Maki-Arvela, P. *et al.*, 2017; Peters, J. *et al*., 2015).

2.3.2 <u>Hydrodeoxygenation of Bio Oil using Precious Metal Catalysts</u>

With noble metals, including Pd, Rh, Pt, and Ru, investigation has been done using them with acidic supports as bifunctional catalysts (Lu, M. *et al*., 2016). Acid treated carbon, γ-Al_2O_3, SiO_2-Al_2O_3 and others were used as the acidic supports. Studies have been done that show the bifunctional mechanism occurs in the reaction pathway of HDO of guaiacol (GUA), one major bio-oil component containing both one -OH group and one -OCH3 group over noble metal supports on acidic oxide catalysts. These are the ring hydrogenation of GUA into 2-methoxycyclohexanol on the noble metal site and deoxygenation of the same 2-methoxycyclohexanol and products. Comparing commercial Pd/γ-Al_2O_3 and CoMoS/γ-Al_2O_3 in GUA HDO, it was found that the Pd/γ-Al_2O_3 was the more active, but catechol was formed. Investigation into HDO of anisole

and GUA over Pt/γ-Al$_2$O$_3$ and Pt/HY catalysts showed that there were significant effects

caused by the acid center types on transalkylation activity of catalysts. Combined effects

of Pd and Fe improved acidity and simultaneously kept the high selectivity to HDO

products with no change to ring saturation or ring opening. Palladium has seen the

widest use as an active metal with HDO catalysts. The electronic and morphological

properties of palladium are in fact predisposed by contact with the support and these

properties show strong effects on the hydrogenation activity of the catalysts. When

reduced at high temperatures, Pd/TiO$_2$ catalytic performance was changed by interaction

between Pd and TiO$_2$ (Lu, M. *et al.*, 2016).

2.3.3 Hydrodeoxygenation of Bio Oil using Other Catalysts

Alternative hydrotreating catalysts were examined include transition metal

phosphides, carbides, nitrides, and rhenium (Zhou, M. *et al.*, 2017). They have

outstanding HDS and HDN performance so are considered suitable s for bio oil HDO

upgrading. These catalysts allow the reduction of HDO cost for bio oil conversion to

fuels and chemicals. Main products of metal phosphides used in conjunction with HDO

include benzene, phenol, and anisole. Drawback of using these catalysts is fast

deactivation (Lu, M. *et al.*, 2016).

2.3.4 Hydrodeoxygenation of Bio Oil Pathways

Because bio oils are a multipart blend of chemical moieties, model compounds

were often used to evaluate the HDO catalyst performance as well as the kinetics,

deactivation mechanism, and reaction pathways GUA is a good representation of

phenolic compounds with its two most common oxygenated groups (hydroxy and

methoxy groups to the benzene ring) widely presented in bio-oil molecules derived from

lignin (Zhou, M. *et al*., 2017). For GUA HDO process, there are two main deoxygenation methods proposed. One is GUA hydrogenation-deoxygenation, that is, hydrogenation happens followed by oxygen removal from saturated hydrocarbon rings. The other one is a direct deoxygenation route, in which C-O-C and C-OH bonds are directly cleaved from the benzene ring without any ring saturation.

Investigation has been done for the hydrodeoxygenation of guaiacol to yield cyclohexanol on non-noble metal catalysts supported on γ-Al_2O_3 and ZSM-5 with a Si/Al ratio of 25 and 38 (Zhou, M. *et al.*, 2017). Better catalytic activity was seen with the Ni/γ-Al_2O_3 catalysts while adding Co for guaiacol conversion to cyclohexanol became the preferred HDO route. Synergistic effects were studied of the active metal moieties and the catalyst support (Zhou, M. *et al.*, 2017). Partial HDO activity is exhibited by HDS catalysts NiMo and CoMo, but again this causes much sulfur contamination and catalyst deactivation. It has been shown that successfully cleaving the aromatic-oxygen bond with Pt/C catalyst is much easier than using Ru, Rh, and Pd on carbon catalyst and yields phenol at greater than 40% using atmospheric pressure, proven stable and as a good catalyst for deoxygenation of guaiacol (Gao, D. *et al*., 2015).

CHAPTER 3

LIGNIN DEPOLYMERIZATION IN SUPERCRITICAL ETHANOL OVER ZEOLITES WITH DIFFERENT ACIDITY AND POROUS STRUCTURES

3.1   Introduction

Lignin is a mixture of natural polyaromatics with several basic phenol units (i.e., coumaryl, coniferyl, and sinapyl) randomly while repeatedly cross-linked mainly with ether linkages. Contributing 20-40 wt.% of mass and ~40% heating value of biomass, lignin, however, has long been a high-volume by-product and environmental hazard of paper and pulp plants. Depolymerization of lignin may not only mitigate such waste and pollution, but also generate great profit by producing high-value aromatic feedstock and/or high-quality fuels. Progress has been made in lignin depolymerization with processes like hydrolysis or thermal cracking to release its rich phenol-type aromatics. Catalysts have been introduced to help improve the cleavage efficiency of C-O-C and C-C linkages of lignin as well as the yield and selectivity of its diverse products. Further studies found that the physical and chemical properties of these catalysts, namely their various acidity and pore structure, play important roles on lignin depolymerization. Similar to what happen in traditional fossil fuel cracking processes, zeolites are widely used in lignin depolymerization, serving either as the catalyst or catalyst support. Their tailorable acidity and uniform pore size make them favorable to achieve better cracking efficiency and product selectivity. However, the unique micropore structure of

traditional zeolites (< 2 nm in diameter) well defined by their crystal framework makes the diffusion of gigantic molecules such as lignin fragments, their oligomers, or even the decomposed monomers difficult, resulting in quick pore blocking, coke formation, and catalyst deactivation. Introducing mesopores (2-50 nm in diameter) or staged hierarchical porosity (i.e., connected macropores, mesopores, and micropores) is considered a promising solution to overcome such limited molecule transport challenges and low active site utilization issues for zeolites in both traditional petrochemical processes and the emerging bio-energy processes like lignin depolymerization.

In this chapter, we investigated the importance of the solid acidity and mesoporous structures of zeolites on catalytic depolymerization of lignin in supercritical ethanol. Compared to other lignin depolymerization processes, ethanolysis under supercritical conditions (scEtOH) is favorable with benefits on high lignin conversion and minimum char formation. Three different types of zeolites with exclusive micropores, HZSM-5, HBeta, and HY, were evaluated, with the first two carry similar micropore size (ZSM-5: 6.36 Å; Beta: 6. 68 Å) and the last two exhibit similar solid acidity (Beta and Y types), as shown in Figure 3-1a. The contribution of mesopore structure, including our special synthesized fin-like and commercial worm-like mesoporous structure in zeolites, was also explored to further reveal its important roles on the cleavage of C-O-C and C-C bonds during scEtOH lignin depolymerization (Figure 3-1b).
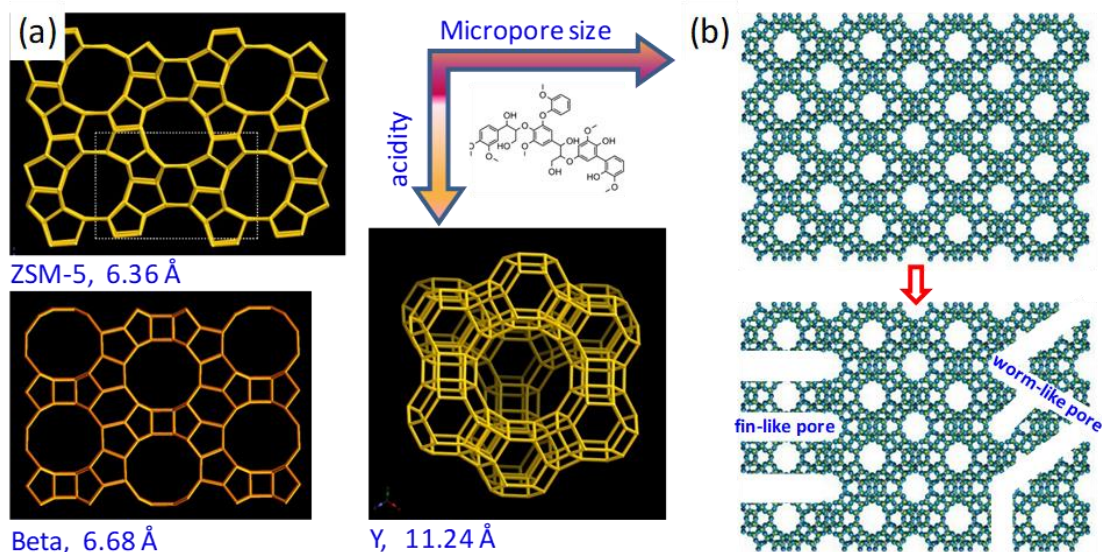
Figure 3-1: Schematics of the framework of ZSM-5, Beta and USY zeolites (a) and a combination of micropore and mesopore (including fin-like pore and worm-like pore) structure (b) that are used in the investigation on the importance of acidity and mesopores during lignin depolymerization in supercritical ethanol process.

3.2   Materials and Methods

3.2.1   Materials

Tetrapropyl ammonium hydroxide (TPAOH, 1 M in H_2O), sodium aluminate ($NaAlO_2$, ~8% H_2O, >99%), aluminium iso-propoxide (AlP), tetramethylammonium hydroxide (TMAOH, 25% aqueous solution), tetraethylorthosilicate (TEOS, >99%), Sodium hydroxide (NaOH) pellets, ethanol ($C2H5OH$, >99.5%), Dimethyloctadecyl[3-(trimethoxysilyl)propyl]ammonium chloride (TPOAC), and cetrimonium bromide (CTAB, >99%) were purchased from Sigma-Aldrich and used as received without further purification. Mesoporous HY zeolites (CBV 720) were purchased from Zeolyst, Inc with a SiO_2/Al_2O_3 ratio of 30.

3.2.2   Zeolite Synthesis

3.2.2.1   ZSM-5 and Fin-Like Mesoporous ZSM-5 Synthesis

For fin-like mesoporous zeolite FM-ZSM-5 synthesis, TEOS, NaAlO$_2$, and TPAOH were firstly added under vigorous stirring with a pre-calculated ratio of TPOAC and CTAB until a clear solution was obtained. The final molar composition of synthesized solution was SiO$_2$: Al$_2$O$_3$: TPAOH: TPOAC: CTAB: H$_2$O=30: 1.0: 6.0: 0.6: 2400. The mixture was further stirred for 2 h at room temperature and then transferred to Teflon lined autoclaves and kept at 150 °C for 48 h. After crystallization, the solid product was separated by centrifugation at the speed of 2,000 rpm for 10 minutes. The received zeolites were further washed several times with distilled water, dried over night at 120 °C, and calcined in air at 550 °C for 8 h. The conventional microporous zeolite ZSM-5 was also synthesized through a similar hydrothermal process aforementioned, but without adding TPOAC and CTAB.

3.2.2.2   Y Zeolites Synthesis

Zeolite Y was prepared in the following method. A solution of 0.05 N NaOH was first prepared and TMAOH and AIP were then added in the same order under vigorous agitation until a clear solution was formed. TOES was then added drop wise and the mixture was aged for 3 days under vigorous stirring at room temperature. This gives a final molar composition of SiO$_2$: Al$_2$O$_3$: Na$_2$O: (TMA)$_2$O: H$_2$O=1: 0.29: 0.0094: 0.72: 108.82. After loading in the aged solution, the Teflon-lined stainless-steel autoclave was sealed and kept at 100 °C for 6 days. After crystallization, the solid product was recovered by centrifugation and further washed with DI water, dried overnight, and calcined in air.

3.2.2.3   <u>Ion-Exchange and H-type Zeolites Preparation</u>

All received sodium type zeolites were first dried and calcined in air at 550 °C for 8 h.

They were then ion-exchanged three times with a 0.1 M NH4NO3 solution at 90 °C for

90 min with a liquid/solid ratio of 10 cm^3/g under magnetic agitation (500 rpm). The

solid was further separated, extensively washed with DI water, and dried over night at

120°C. The dried zeolite samples were finally calcined at 550 °C for 6 h with a

temperature ramp rate of 1.5 °C/min to receive H-type zeolites.

3.2.3   <u>Characterization</u>

3.2.3.1   <u>Scanning Electron Microscopy (SEM) Imaging</u>

SEM images were taken on a Hitachi S-4800. Samples were prepared by dusting

the zeolite powder onto double sided carbon tape and mounted on an alumina stub. All

samples were subsequently sputter coated with a thin gold film to reduce charge effects.

3.2.3.2   <u>X-ray Diffraction (XRD)</u>

XRD analysis was done on a Bruker D8 diffractometer, using Cu-Kα radiation at

room temperature and instrumental settings of 40 kV and 40 mA. Data were recorded in

the 2θ range of 6–55º with an angular step size of 0.02º.

3.2.3.3   <u>Surface Area and Porosity Analysis</u>

Nitrogen adsorption isotherms were obtained at -196 °C on a Micromeritics

ASAP 2020 Surface Area and Porosity Analyzer in a relative pressure range from 0.05 to

0.99. Before measurement, samples were degassed at 300 °C for 6 h. The pore size

distribution was calculated using the Nonlocal Density Functional Theory (NLDFT)

method from the adsorption branch.

3.2.4   <u>Lignin Depolymerization Tests</u>

The catalytic conversion of Kraft lignin was carried out at 280 °C for 6 h in a

high-pressure batch reactor (Col-Int Tech, 200 mL). For each run, 1.0 g lignin, 0.5 g

catalyst, and 100 mL ethanol were first loaded in the reactor and the sealed reactor was

then evacuated and purged with high-purity nitrogen gas for three times at room

temperature. The reactor temperature was then risen to 280 °C with the reactor pressure

reaching ~8 MPa. After the reaction was carried out for 6 h, the liquid was filtered and

taken for product identification and analysis on a gas chromatography-mass spectrometry

(GC-MS) instrument (Agilent 7890A-5975C). Benzyl alcohol (0.1 vol% in ethanol, 1.0

µL) was added in the product samples (1 mL) before GC-MS analysis, serving as the

known internal standard in GC-MS spectra to normalize the peak area for each

compound. Multiple-point internal standard plots were generated, covering the expected

concentration range of major product compounds. For those commercially available

compounds, such as 4-methyl phenol (i.e., cresol) and 2-methoxy-phenol (i.e., guaiacol),

diluted solutions with known concentrations were prepared. For other commercially-not-

available compounds such as 3-methyl-1- adamantaneacetic acid, the lignin

depolymerization product obtained from different catalysts was mixed and further

concentrated by evaporating most ethanol using a rotary evaporator. The obtained liquid

was then diluted with ethanol to get different concentrations of each compound using

benzyl alcohol as the internal standard (0.8 mM). Plots of the peak area ratio of several

major aromatic compounds in lignin depolymerization products to the internal standard

(benzyl alcohol) were made versus the concentration ratio (Wang, Y., *et al.* 2017). The

original concentrations of those commercially-not-available compounds in the mother

solution were determined by their area ratios to guaiacol whose concentration in samples was found through their own multiple-point internal standard curve.

3.3   Results and Discussion

3.3.1   <u>Morphology and Textural Properties of Zeolites Used in Lignin Depolymerization</u>

The texture properties of different types of zeolites used in lignin depolymerization in supercritical ethanol were characterized with SEM, XRD, and Pore Size Analyer. Because of their similar synthesis receipt, similar elongated, hexagonal plate shape with an average dimension of ~$225 \times 500 \times 700$ nm was obtained for both microporous ZSM-5 and mesoporous ZSM-5 zeolites, as shown in Figures 3-2a & 3-2b. But rather than conventional microporous ZSM-5 zeolites that exhibit smooth surface on each axis direction, the morphology of mesoporous ZSM-5 obtained with the assistance of dual meso-templates is quite different. Multiple laminar structures are shown in the b-axis direction of mesoporous ZSM-5 zeolites which are fused together in one end on the a-axis framework into a large monolithic piece to create fin-like mesoscale space (Figure 3-2b). The XRD patterns of mesoporous ZSM-5 and common microporous ZSM-5 samples show identical, well-resolved peaks which belong to MFI zeolite structure (Figure 3-2c). This confirms the successful synthesis of ZSM-5 with this new fin-like mesoporous structure (denoted as FM-ZSM-5 in later discussions). Their different pore structures are further confirmed through the N_2 adsorption–desorption isotherms. As shown in Figure 3-2d, conventional microporous ZSM-5 presents a classic type I adsorption/desorption isotherm for microporous materials, which has only one high uptake at low relative pressure (P/P0 < 0.02) and a long plateau in the high-pressure

range (0.4 < P/P0 < 0.9), indicating that the material is a purely microporous phase with negligible mesoporosity. On the contrary, FM-ZSM-5 zeolites present a combination of both type I and type IV(a) adsorption/desorption profiles with two steep uptake steps, one at P/P0 < 0.02 and the other at 0.45 < P/P0 < 0.90 locations, responding for micropore filling and mesopore capillary condensation, respectively (Figure 3-2d). The disappearance of hysteresis loop on the adsorption–desorption isotherms of typical mesoporous materials at high relative pressure further confirm the existing of uniform, one end open, fin-like mesopore structure in this new FM-ZSM-5 zeolites. Although the use of traditional BET approach to extract surface area and pore volume information contributed by micropores from these N_2 adsorption–desorption isotherms is known questionable for most zeolites, such results serve as valuable reference in comparisons. The textural parameters (Table 3-1) further reveal that FM-ZSM-5 has evidentially larger BET surface area (460.3 m^2/g vs. 354.3 m^2/g), larger pore volume (0.32 cm^3/g vs. 0.24 cm^3/g), and larger average BJH pore size (3.6 nm vs. 2.7 nm) when compared to its microporous counterpart.

Table 3-1: Textural Properties of Microporous and Mesoporous HY and HZSM-5 Zeolites

Sample	S_{BET} (m²/g)	S_{Micro}[a] (m²/g)	S_{ext}[a] (m²/g)	V_{total}[b] (cm³/g)	V_{Micro}[a] (cm³/g)	V_{Meso} (cm³/g)	Pore Size[c] (nm)
H-ZSM-5	354.3	222.2	132.2	0.24	0.08	0.16	2.7
Meso-HZSM-5	460.3	87.8	372.5	0.32	0.03	0.29	3.6
H-Y	720.6	566.1	154.5	0.33	0.21	0.07	2.6
Meso-HY	766.3	410.5	355.8	0.50	0.15	0.22	6.9

[a] t-Plot Micropore Area; [b] Single point total pore volume at P/P0 = 0.98; [c] BJH Desorption average pore.
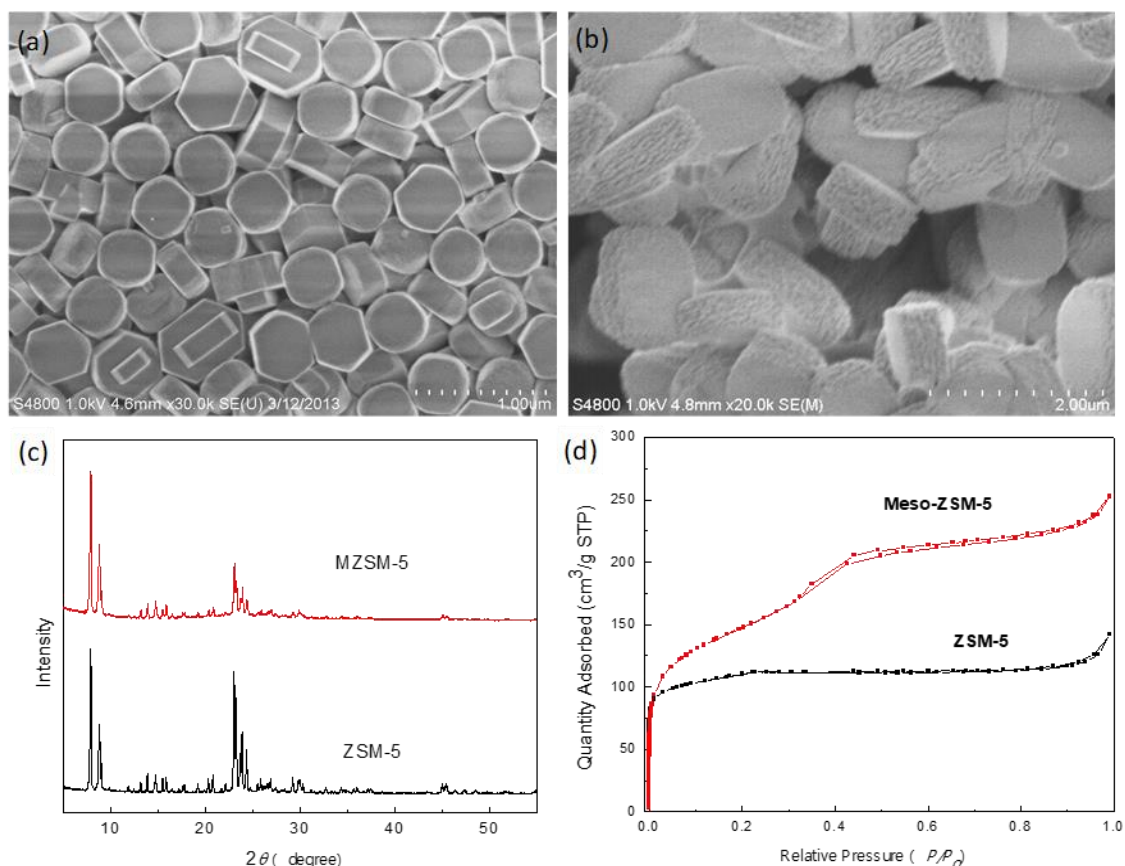
Figure 3-2: SEM images of ZSM-5 (a) and FM-ZSM-5 with fin-like mesoporous structure (b), XRD patterns (c) and N_2 sorption isotherms (d) of FM-ZSM-5 and ZSM-5 zeolites.

Similar morphology and texture properties of microporous HY and mesoporous HY (denoted as Meso-HY in later discussions) zeolites were also measured. As shown in Figures 3-3a-3-3c, similar crystal sizes (400-500 nm) and identical XRD patterns are found for Meso-HY and microporous HY zeolites used in this lignin depolymerization study. But unlike FM-ZSM-5 with fin-like mesopores, Meso-HY zeolites show worm-like mesoporous structure (Figure 3-3b). Their hierarchical pore structure is also quantified through N_2 adsorption–desorption isotherms. As shown in Figure 3-3d, conventional microporous HY zeolites present a classic type I adsorption/desorption isotherm for microporous materials, which has only one high uptake at low relative

pressure (P/P0 < 0.02) and a long plateau in the high-pressure range (0.4 < P/P0 < 0.9).

On the contrary, Meso-HY zeolites present a combination of both type I and type IV

adsorption/desorption profiles with two uptake steps, a steep one at P/P0 < 0.02 followed

by a slow one afterward, responding for micropore filling and mesopore capillary

condensation, respectively. A hysteresis loop at 0.45 < P/P0 < 0.90 locations suggests the

existence of hierarchical pore structure in Meso-HY zeolites. The textural parameters

given in Table 3-1 confirms evidentially larger BET surface area (766.3 m^2/g for Meso-

HY vs. 720.6 m^2/g for HY), larger pore volume (0.50 cm^3/g for Meso-HY vs. 0.33 cm^3/g

for HY), and larger average BJH pore size (6.9 nm for Meso-HY vs. 2.6 nm for HY) of

Meso-HY than its microporous counterpart. Although BET method underestimates the

contribution of micropores to the total surface area of zeolites, its accuracy on

mesoporous structure measurement confirms the availability of many mesopores in

Meso-HY zeolite crystals. As shown in Table 3-1, more overall surface area is accessible

to probe molecules (i.e, N_2) contributed by the addition of mesopores according to the

BET method calculation, despite the reduction of the surface area contributed by

micropores. For the same reasons (i.e., introduction of mesopores), the calculated pore

volume and average pore size in Meso-HY also significantly increased (Table 3-1).
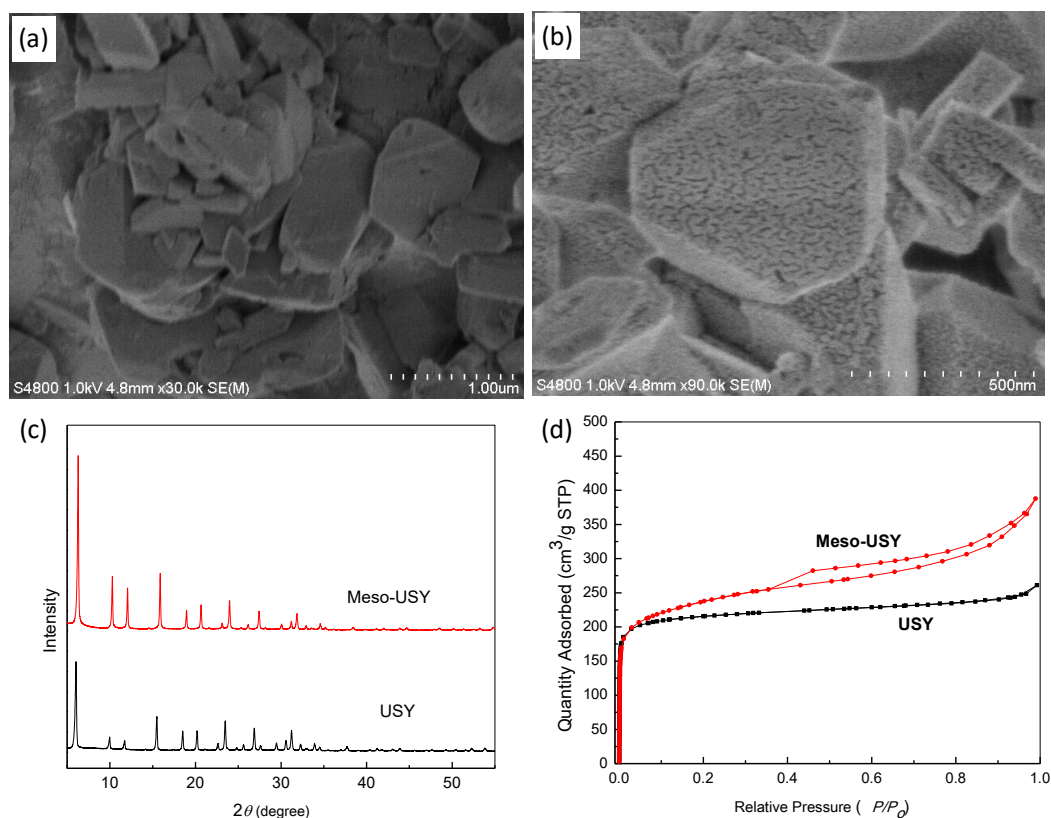
Figure 3-3: SEM images of microporous HY zeolite (a) and Meso-HY zeolite with worm-like mesoporous structure (b). XRD patterns (c) and N_2 sorption isotherms (d) of microporous HY and Meso-HY zeolites.

3.3.2   Importance of Pore Size and Acidity of Microporous Zeolites in Lignin

Depolymerization

To investigate how important the pore size and acidity of different microporous

zeolites for Kraft lignin depolymerization in supercritical ethanol, three types zeolites,

HZSM-5, HBeta, and HY zeolites with exclusive micropores were chosen to study here.

These zeolites are widely used in fossil fuel processes, in which the first two carry similar

micropore size (HZSM-5: 6.36 Å; HBeta: 6. 68 Å) but different acidity while the last two

have similar solid acidity (HBeta and HY types) but different micropore size (HBeta: 6.

68 Å; HY: 11.24 Å), as shown in Figure 3-1a. The catalytic depolymerization of Kraft

lignin was carried out in a batch reactor after purging with N_2 prior to elevating the

reaction temperature and pressure to what were used in our previous research work (i.e.,

at 280 °C under a pressure of 8 MPa for 6 h). All three types of zeolites exhibit high

lignin conversion (65-75%) with very little char formation, consistent with previous

findings using supercritical alcohols. More than 20 product molecules with a mass weight

of more than 1.0% were detected by GC-MS in the liquid product samples, as shown in

Figure 4a. The early eluted C_4-C_6 products in the GC-MS spectrum are some short-chain

ether (e.g., 1,1-diethoxy-ethane as one dominant peak), ester (e.g., ethyl acetate as one

dominant peak), alcohols (e.g., butanol as one dominant peak), fatty acid (e.g., acetate),

or acetal (e.g., butanal as one dominant peak) that derivate from ethanol reforming

reactions at the presence of zeolites. This is verified when comparing the GC-MS

spectrum of lignin ethanolysis products with that from a blank test involving only ethanol

and zeolites at the same reaction conditions (Figure 3-4). Compounds eluted after 7
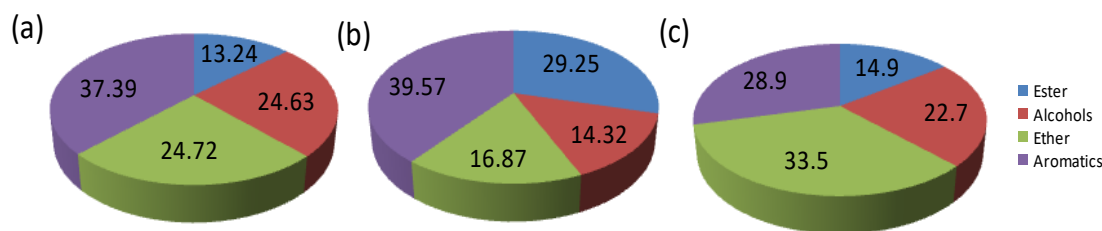
minutes, including different alcohols, esters, and aromatics, appeared only when lignin

was added (Figure 3-4). The product molecules are similar in all ethanolysis samples

catalyzed by the three different types of microporous zeolites. But the yield and

selectivity of individual products or a group of compounds was quite different. Aromatic

products were found much higher in samples depolymerized by microporous HZSM-5

and HY than HBeta zeolites (HZSM-5: 37.4%; HY: 39.6%; HBeta: 28.9%), as shown in

Figures 3-5b-3-5d. Considering the relatively smaller size of micropores in HZSM-5 and

HBeta than in HY, it seems that the diffusion issues caused by micropore size play a

more important role on the aromatic production than their solid acidity, given the similar

micropore size while different acidity of HZSM-5 and HBeta zeolites. Signals of the later

eluted C_8-C_{11} compounds, most as aromatics, became more diverse for samples

depolymerized over HBeta and HY than HZSM-5 (Table 3-2 and Figure 3-4). These

results suggest that zeolites with strong acidity (e.g., HY and HBeta) work better to break

down C-O-C (e.g., β-O-4) and C-C (e.g., β-1) linkages in lignin structure into small

phenolic molecules. With both large micropores and strong acidity, it is not a surprise for

microporous HY zeolites to receive the highest selectivity on phenols and the most

diversified aromatic products (Table 3-2 and Figure 3-4).

41
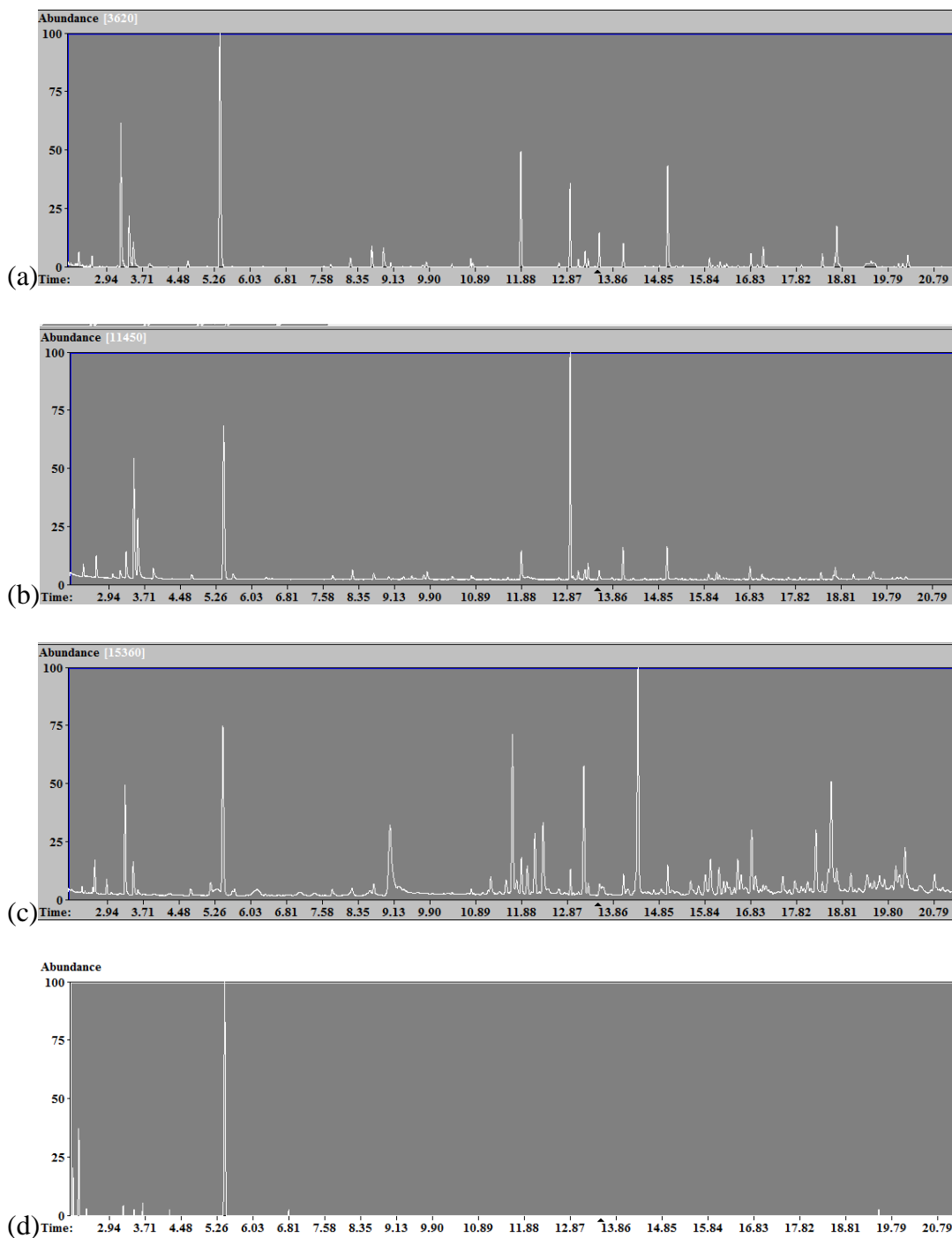
Figure 3-4: GC-MS spectra of lignin depolymerization in supercritical ethanol with microporous HBeta (a), HZSM-5 (b), HY (c), and a blank test (with only ethanol and HZSM-5, no lignin) (d).

Figure 3-5: Classified product distributions of lignin catalytic depolymerization in supercritical ethanol over microporous HZSM-5 (a), HY (b), and HBeta (c) zeolites

3.3.3 Zeolites with Different Acidity while Same Micropore Structure in Lignin

Depolymerization

In aforementioned comparison, though two zeolite types (i.e., HZSM-5 and HBeta) have similar micropore structure while the other pair (i.e., HY and Hbeta) have similar acidity, they have framework differences among their crystal structure. To rule out that complexity, we further looked into how solid acidity affects the scEtOH lignin depolymerization under the same microporous structure. As well-known zeolites gain their solid acidity through transforming from sodium type to H types by multiple ion-exchange processes, we prepared zeolites with different acidity while the same microporous structure by regulating the replacement level of sodium in their crystal structure. We ion-exchanged once the fresh synthesized microporous Y zeolites (designated as NaNH$_4$Y in later discussions) and compared how this partially ion-exchanged zeolites performed in scEtOH lignin depolymerization with their exclusive sodium type (denoted as NaY) and fully-ion exchanged H-type counterparts (denoted as HY). As shown in Figure 3-7a, the NaY zeolites gives a yield of 16.1% aromatics of all depolymerization products, which increases to 29.8% when using the ion-exchanged once zeolites (NaNH$_4$Y) and to 39.7% with fully ion-exchanged HY zeolites, respectively. Among all aromatic products, more phenols are received when increasing the solid
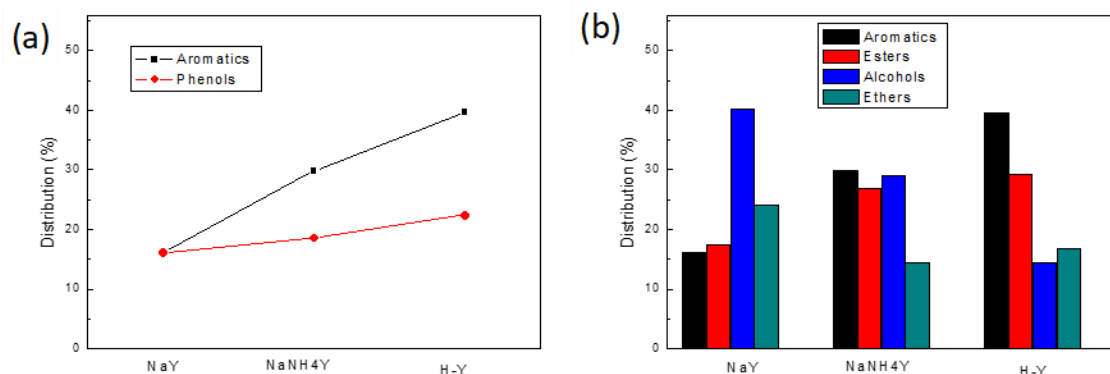
Figure 3-7: (a) Aromatics and phenol, (b) all products of supercritical ethanol depolymerization of lignin over Y zeolites with different acidity but the same microporous structure

3.3.4   Importance of Mesopores to Zeolites in Lignin Catalytic Depolymerization

Generally speaking, micropores defined by the crystal framework of zeolites are too small for lignin fragments and its excessive intermediate oligomers or monomers to diffuse deep into zeolite crystals to reach numerous acidic sites over there. This causes those giant molecules to largely accumulate near the entrance of micropores close to surface, which eventually block them and form coke there. This quickly deactivates the zeolites catalyst just like what exclusively happens in fossil fuel cracking processes. Mesoporous zeolites or zeolites with a network of pores at different scales (i.e., hierarchical pore structure) are therefore necessary to improve the transport of bulky reactants or products inside zeolites. Even although the introduction of mesopores in zeolite crystals might reduce the surface area contributed by micropores if those mesoscale space was originally part of zeolite framework, their presence provides more accessible surface area: not only the new surface area created by mesopores, but also more accessible surface from micropores deep inside zeolite crystal. Besides, the availability of mesopores also helps expose and utilize more acidic active sites inside

zeolite crystals. To reveal how mesopores contribute to lignin conversion and aromatic selectivity, we compared the catalytic cracking performance of HZSM-5 and HY zeolites with exclusive micropores and those having a combination of micropores and mesopores in scEtOH lignin depolymerization. As shown in Figure 3-8 and Figures 3-9a-3-9b, signals of compounds of C_8-C_{11} eluted later than 7 minutes in the GC-MS spectra increase greatly for samples that were depolymerized by FM-HZSM-5 than that using microporous HZSM-5. Although having a complex products, the dominant products include fatty acid esters and aromatics. But the signal increase of the former (i.e., fatty acid) is much less than the latter (i.e., aromatics, mainly involving phenols). The high yield of aromatics (65.4% for FM-HZSM-5 versus 37.4% for HZSM-5) with more diversified individual aromatic compounds suggests deeper breakdown of lignin fragments over FM-HZSM-5 (Figures 6a-6b). Among all aromatic products, there is one major aromatics in lignin ethanolysis products over both types of HZSM-5 zeolites, 1,2-Dimethoxy-4-(1-methoxyethenyl) benzene (43.9% for FM-HZSM-5 versus 25.4% for HZSM-5), a relatively large intermediate aromatic fragment. Desired phenols including guaiacol and alkane substituted guaiacols such as methyl- and ethyl- substutited guaiacols have obviously high yield over FM-HZSM-5 catalyst (~21.5%) than microporous HZSM-5 (~12.0%), as shown in Table 3-2. The higher phenol selectivity over FM-HZSM-5 zeolites is attributed to their unique textural features which promote the lignin depolymerization from two aspects: (i) its fin-like configuration creates many mesoscale pathways that significantly reduce the diffusion resistance for large molecules to reach and leave the connected micropores in zeolite crystal to avoid pore blocking and coke formation; (ii) such more open configuration also help expose more crystal surface,

micropores, and the acidic sites inside zeolite crystal, making them accessible to bulky molecules (e.g., partial depolymerized, intermediate molecules) so that they can interact with the active sites of zeolites, get further cracked into small molecules (e.g., phenols) before leaving zeolite surface. With more aromatics produced, the percentages of alcohol, ester, and ether in the liquid product all drop for samples treated over FM-HZSM-5 zeolites (Figures 3-9a-3-9b).
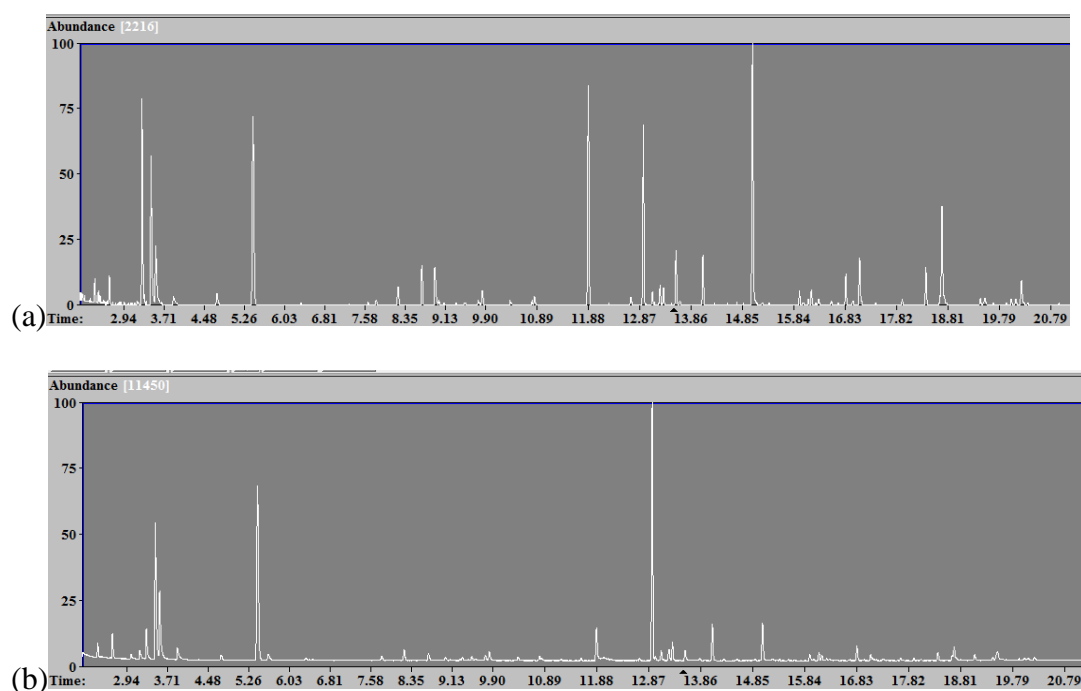
Figure 3-8: GC-MS spectra of lignin depolymerization in supercritical ethanol with mesoporous FM-HZSM-5 (a) and microporous HZSM-5 (b) zeolites
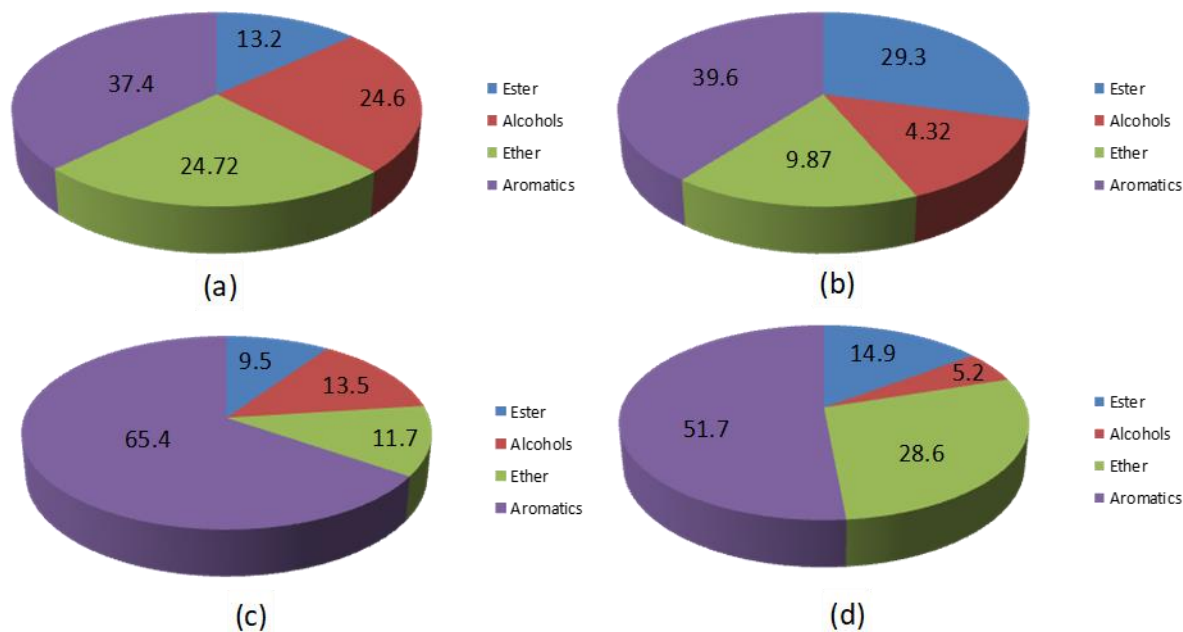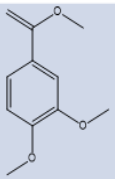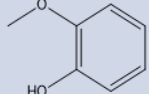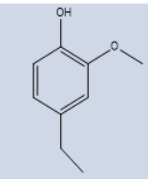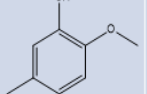
Figure 3-9: Classified product distribution of supercritical ethanol depolymerization of lignin over with different zeolites: (a) HZSM-5, (b) FM-ZSM-5, (c) HY, (d) Meso-HY

Like the scEtOH lignin depolymerization over ZSM-5 zeolites, HY and Meso-HY zeolites contribute similar depolymerisation products that are assigned to aromatics, ester, alcohol, and ether of C_4-C_{12}. However, the distributions of product compounds in each group are quite different: the ether percentage in all liquid products increases despite the yields of alcohol and ester drop (Figures 3-9c-3-9d). This might be the result of quick transformation reactions between many side groups cleaved from lignin structure and the availability of deprotonated ethanol molecules under supercritical state. As for aromatics, similar increase on the yield of aromatics (51.7% for Meso-HY versus 39.6% for HY) and more diversified individual compounds (Table 3-2) when mesopores were introduced suggest deeper breakdown of lignin over Meso-HY than over microporous HY (Figures 3-9c-3-9d). This again endorses the two major contributions of mesopores to the scEtOH

lignin depolymerisation discussed early about HZSM-5 and FM-HZSM-5: lower diffusion resistance and more exposed acidic sites inside zeolites.

Table 3-2: Aromatics Selectivity of Lignin Depolymerization Product over Zeolites with Microporous and Mesoporous Structures

Catalyst	Aromatics Selectivity	Main Aromatic Products				
						others
HBeta	28.9	7.8	11.2	5.5	-	3.4
HY	39.6	17.2	10.9	5.9	2.6	3.0
HZSM-5	37.4	25.4	4.2	2.5	1.3	4.0
FM-HZSM-5	65.4	43.9	9.9	4.4	1.6	5.6
Meso-HY	51.7	8.1	13.3	13.3	1.7	15.3

As for aromatics, lower yield of gigantic intermediate products such as 1,2-Dimethoxy-4-(1-methoxyethenyl)benzene was found for samples treated with both types of Y zeolites when compared to what over HZSM-5 zeolites (HY: 17.2%, Meso-Y: 8.1% vs. HZSM-5: 25.4%, FM-ZSM-5: 43.9%), as shown in Table 3-2. Among all aromatic products, more phenols were found in lignin depolymerization products over Y zeolites (HY: 22.4%, Meso-Y: 37% vs. HZSM-5: 12.0%, FM-ZSM-5: 21.5%). This suggests that the strong acidity of Y zeolites promotes not just the ether linkages (e.g., β-O-4 bonds) on the benzene ring of lignin structure, but also the C-C linkages (e.g., β-1 bonds), particularly those connecting the benzene ring and the fatty acid side group like para-

adamantaneacetic acid groups in 1,2-Dimethoxy-4-(1-methoxyethenyl)benzene. This finding is consistent with what happened in EtOH lignin depolymerisation involving other zeolites with strong acidity. For examples, in Table 3-2, for depolymerisation samples using HBeta and HY, their yield of 1,2-Dimethoxy-4-(1-methoxyethenyl)benzene is lower than that using HZSM-5 (HY: 17.2%, HBeta: 7.8%, HZSM-5: 25.4%). As the consequence, the types and yields of phenols (i.e., guaiacol and alkane substituted guaiacols) and C_8-C_{11} fatty ethers or esters formed from cleaved side groups are also much higher over those zeolites with stronger acidity (Table 3-2 and Figure 3-4). Even for mesoporous zeolites, Meso-HY also contributes more phenol compounds and higher yield of many of them in its lignin depolymerization products when compared to FM-HZSM-5 with fin-like mesoscale pathways (Table 3-2). These results further endorse the importance of strong solid acidity of zeolites during scEtOH lignin depolymerization. It helps the deep breakdown of lignin fragments and higher selectivity to small phenolic aromatics. Because of the scEtOH lignin depolymerization complexity, the contribution difference between various mesopore structures seem not sensitive to the product distribution changes when compared to their acidity impact. With the diffusion of gigantic molecules less restricted to reach the surface of zeolites, the number of strength of the acidic sites on zeolites decide the eventual cracking levels of lignin and its large intermediate such as 1,2-Dimethoxy-4-(1-methoxyethenyl)benzene to small molecules (e.g., phenols) before leaving the catalyst surface.

3.4 Conclusion

In summary, we examined how acidity and pore structure of different zeolites play on lignin depolymerization in supercritical ethanol. Zeolites with similar micropore size

(HBeta and HZSM-5) or acidity (HBeta and HY) defined by their crystal structures were first used to evaluate the roles of these two important factors in lignin depolymerization. Zeolites with the same microporous structure, but different acidity caused by various ion-exchange degrees were further evaluated, followed by zeolites with similar acidity but different pore sizes (i.e., mesoporous zeolites versus and microporous counterparts of HZSM-5 and HY zeolites). Despite the complexity of lignin depolymerization and its greatly diversified products, the strong acidity in HBeta and HY was found effective to cleave both C-O-C and C-C linkages in lignin structure to receive more phenols while HZSM-5 with mild acidity break down mainly the ether bonds. Hierarchically porous structure is important to promote mass transport and the exposure and utilization of the acidic sites inside zeolites like in many petrochemical reactions involving bulky molecules. But when the diffusion issues become less severe for bulky lignin and its partially decomposed intermediate and monomer compounds (e.g., in mesoporous zeolites), the acidity dominantly decides the yield and selectivity of lignin depolymerization product. These findings provide important guidelines on the selection and design of zeolites with appropriate acidity and porous structure to facilitate the scEtOH depolymerization of lignin, which will help not only eliminate this high-volume farm waste and environmental hazard of paper and pulp plants, but also to promote the utilization efforts on converting its rich aromatic units into important chemicals and fuels. The same knowledge could also benefit other catalytic cracking processes using a variety of heating and/or solvent assistance to improve the conversion, yield, and selectivity of bulky hydrocarbons.

CHAPTER 4

HYDRODEOXYGENATION OF DEPOLYMERIZATION COMPONENTS OVER PALLADIUM/MESOPOROUS ZEOLITES

4.1 Introduction

Pyrolysis bio-oil is a mixture of various organic compounds including alcohols, sugars, furans, phenols, and other large hydrocarbons. It retains up to 70% of the total energy of the abundant raw biomass and serves as one of the most promising alternative or replacement to fossil fuel (Talmadge, M. S. *et al.* 2014; Shi, Y., *et al.* 2017). However, its direct use in conventional combustion engines is unfavorable due to its high oxygen content (up to 40 wt.%), poor thermal stability, and low heating values (16-19 mJ/kg) (Hernando, H., *et al*. 2016; Wang, Y., *et al*. 2012). Hydrotreating step, a classic refinery process to remove oxygen, sulphur, nitrogen, and other unwanted elements in oil by adding hydrogen, is often suggested for the upgrading of bio-oil to increase its C/O ratio, improve its energy density, stability, as well as other required fuel properties (Wang, Y., *et al*. 2011; Wang Y., *et al*. 2014). As bio-oil has low or none sulfur-containing compounds, conventional hydrotreating catalyst (i.e., NiMoS and CoMoS) are undesired due to their inevitable introduction of sulfur into the hydrodeoxygenation (HDO) products and consequent extra removing process. Their high operation temperature (i.e., 350 °C or higher) is also unfavorable for bio-oil HDO, easily leading to the formation of heavy hydrocarbons and coke that quickly deactivate the catalyst (Griffin, M. B., 2017;

51

Lai, Q., *et al.* 2017; Kordouli, E., *et al.* 2017; Sun, J., *et al.* 2013; Zhao, H. Y., *et al.* 2011; Olcese, R. N., *et al.* 2012). Noble metals (Pd, Pt, and Ru) catalysts, on the other hand, exhibit excellent hydrotreating performance in the removal of oxygen and/or saturation of hydrocarbons at relatively low reaction temperature (Zhao, C. *et al.* 2012; Zhu, X., *et al.* 2011; Bjelic, A., *et al.* 2019; Bjelic, A., *et al.* 2019). Beside the superior hydrogenation function of noble metal, the acidity and pore structure of catalyst support also play important roles on the overall catalyst activity through improving metal dispersion as well as enhancing adsorption and/or diffusion of reactive specie (Infantes-Molina, A. *et al.* 2015; Hunns, J. A. *et al.* 2016; Wang, Y., *et al.* 2013). Among different supports, zeolites are often adopted for their uniform pore structure and strong acidity (Sotelo-Boyas, R., *et al.* 2010; Grilc, M., *et al.* 2014). These features help improve the dispersion of noble metal clusters, enhance metal−support interactions, and regulate product selectivity. However, traditional single crystal zeolites carry only micropores defined by their unique crystal framework, which causes great diffusion resistance for large reactant/product molecules and high risk of coking formation. This is particularly unfavorable for bio-oil upgrading due to their inclusion of excessive giant oligomers (Hong, D. Y., *et al.* 2010; Valle, B., *et al.* 2010). Therefore, mesoporous zeolites or zeolites with a network of pores at different scales (i.e., hierarchical pore structure) are desired supports for hydrotreating catalyst in bio-oil upgrading processes which promote both diffusion and overall catalytic performance.

Recently, we developed a new mesoporous zeolite ZSM-5 synthesis route, in which dry aluminosilicate nanogels are transformed into nanocrystal in solid state (Wang, Y., *et al.* 2017). Neighbor developing nanocrystals further joint at edges, creating

connected, inter-lattice mesoscale pathway in the finished single crystalline zeolites. This new mesoporous ZSM-5 zeolite (designated as Meso-ZSM-5) carries the merits of nanocrystal zeolites on mass transport promotion for bulky molecules while avoid their intrinsic drawback on hydrothermal stability. We introduce palladium (Pd) metal over this new mesoporous zeolite ZSM-5 support (designated as Meso-ZSM-5) to form a bi-functional catalyst (designated as Pd/Meso-ZSM-5) and investigated its hydrodeoxygenation (HDO) activity for bio-oil upgrading. Guaiacol (GUA) is selected as the model compound of bio-oil owing to its two oxygenated groups (i.e. methoxy and hydroxyl) widely presented in many pyrolysis oil compounds. Its high oxygen content and easy coke formation issue often leads to disappointed HDO performance over many traditional hydrotreating catalysts, particularly those that are supported on microporous materials (Wang, Y., *et al.* 2012; Choi, M., *et al.* 2006). The HDO of guaiacol was conducted at a temperature of 150-250 °C over Pd/Meso-ZSM-5 and Pd catalyst supported on microporous ZSM-5 to investigate the potential improvement of this new catalyst on guaiacol conversion and anti-coking resistance.

4.2   Materials and Methods

4.2.1   Materials

Tetrapropyl ammonium hydroxide (TPAOH, 1 M in H_2O), sodium aluminate ($NaAlO_2$, ~8% H_2O, >99%), tetraethylorthosilicate (TEOS, >99%), Tetraamminepalladium(II) chloride monohydrate ($Pd(NH_3)4Cl_2 \cdot H_2O$, >98%), and Guaiacol (>99%), were purchased from Sigma-Aldrich and used as received without further purification.

4.2.2   Meso-ZSM-5 Synthesis by Solid-State Crystallization

Meso-ZSM-5 zeolites were synthesized by mixing TPAOH, NaAlO$_2$, TEOS, and H$_2$O with a molar ratio of 0.25TPAOH: 0.015Al$_2$O$_3$: SiO$_2$: 80H$_2$O. TPAOH and NaAlO$_2$ were first dissolved in H$_2$O, followed by adding TEOS under strong agitation. The mixture was kept at 80 °C until a clear solution was obtained, which was left overnight at room temperature for solvent evaporation. The as-prepared dry nanogels were further transferred to a Teflon-lined autoclave for crystallization at 140 °C for 12 h without adding any additional water. Conventional ZSM-5 zeolites with a similar Si/Al ratio of 33 were synthesized via traditional hydrothermal method at 150 °C for 48 h.

The synthesized zeolite samples were ion-exchanged three times with a 0.1 M NH$_4$NO$_3$ solution at 90 °C for 90 min (liquid/solid ratio = 10 mL/g) under stirring. Samples were then filtered, extensively washed with distilled water, and dried at 100 °C for 4 h. H-type ZSM-5 samples were prepared after further calcined in air at 500 °C for 6 h (at a heating rate of 1 °C /min). The hydrothermal stability of zeolites was tested at 150 °C for 72 h in autoclave with a water/zeolite ratio of 50.

4.2.3   Pd/Zeolite Catalyst Preparation

Pd/ZSM-5 and Pd/Meso-ZSM-5 catalysts were prepared by conventional incipient wetness impregnation. In brief, a aqueous solution of Pd(NH$_3$)4Cl$_2$·H$_2$O (10mL, containing 12.4 mg Pd(NH$_3$)4Cl$_2$·H$_2$O) was added dropwise to wet H-type zeolite powder (1.0g) at room temperature and the suspension was further diluted with DI water to a total volume of 50 mL under agitation (200 rpm). After 3 hours of stirring, the suspension was left still, allowing for solvent evaporation. The dried catalyst samples were then transferred to a furnace for further drying at 120 °C for 12 h and calcined at 500 °C for 4

h (with a heating rate of 1.5 °C/min). Dried catalyst samples were reduced in a flow of H_2

for 3 hr at 450 °C, using a heating rate of 2.5 °C/min prior to use.

4.2.4   Characterization

4.2.4.1   X-ray Diffraction (XRD)

        XRD analysis was done on a Bruker D8 diffractometer, using Cu-Kα radiation at

room temperature and instrumental settings of 40 kV and 40 mA. Data were recorded in

the 2θ range of 5–60° with an angular step size of 0.02°.

4.2.4.2   Electron Microscopy (SEM) Imaging

        Scanning electron microscopy (SEM) images were taken on a Hitachi S-4800.

Samples were prepared by dusting the zeolite powder onto double sided carbon tape and

mounted on an alumina stub. All samples were subsequently sputter coated with a thin

gold film to reduce charging effects. Transmission electron microscopy (TEM) and

selected-area electron diffraction (ED) measurements were carried out on a Hitachi H-

9500 high-resolution TEM (HRTEM) instrument operating at 300 kV. The samples were

suspended in ethanol and dispersed on a copper grid coated with lacey carbon film before

TEM analysis.

4.2.4.3   Surface Area and Porosity Analysis

        Nitrogen adsorption isotherms were obtained at -196 °C on a Micromeritics

ASAP 2020 Surface Area and Porosity Analyzer in a relative pressure range from 0.05 to

0.99. Before measurement, samples were degassed at 300 °C for 6 h. The total surface

area of catalyst was calculated according to the Brunauer-Emmett-Teller (BET) method

(Note: the BET method underestimates the specific area of microporous zeolite (Du, X.,

and E. Wu, 2007)). The pore distribution was obtained by the Barrett-Joyner-Halenda (BJH) analysis on the adsorption branch of the isothermal curve.

4.2.4.4 Ammonia Temperature Programmed Desorption (NH_3-TPD) Analysis

The NH_3-TPD was used to measure the acidity of zeolites on a Micromeritics AutochemII Chemisorption Analyzer. Zeolite materials (50 mg) were pretreated at 300 °C for 1 h and then cooled down to 50 °C in an Ar flow of 20 cm^3/min. Pure NH_3 (at a flow rate of 20 cm^3/min) was injected until adsorption saturation, followed by Ar purging for another 1 h. The desorption of NH_3 was monitored in the range of 50–700 °C with a ramp of 10 °C /min by a TCD detector. Hydrogen chemisorption was done on a Micromeritics ASAP 2020C instrument to determine the Pd dispersion on the support. This was done by calculating the difference between the two adsorption isotherms (strong H_2 adsorption) and extrapolating the curves to zero pressure, assuming H/M = 1 at the metal surface.

4.2.4.5 Hydrogen Temperature Programmed Reduction (H2-TPR) Analysis

In H_2-TPR measurement, a 0.2 g catalyst sample was first pretreated at 300 °C for 120 min in a flow of N_2 (30 mL/min). After cooling down to 75 °C, the sample was further heated up to 750 °C at a heating rate of 10 °C/min in a flow of 10% H_2 in argon (30 mL/min). Hydrogen consumption was measured using calibrated TCD signal.

4.2.4.6 Thermo-Gravimetric Analysis (TGA) Analysis

TGA was used to quantify carbon formed on catalyst after reaction using a TGA 2050 Thermogravimetric Analyzer (TA Instruments, Inc). The weight loss of catalyst samples was monitored through a thermal scanning from 20 to 600 °C at a ramp rate of 10 °C/min in air atmosphere.

4.2.5   Guaiacol Hydrodeoxygenation Tests

The hydrodeoxygenation (HDO) of guaiacol over Pd/ZSM-5 and Pd/Meso-ZSM-5 catalysts were evaluated in a high-pressure batch reactor (Col-Int Tech, 400 mL). Guaiacol of 1.0 g was dissolved in n-hexadecane (99%, Sigma-Aldrich) of 100 mL and the solution was loaded in the reactor, together with 0.3 g catalyst. Prior to loading, catalyst was reduced H_2 for 3 hr at 450 °C. The reactor was then sealed tightly and purged three times with first N_2 then H_2 prior to being heated to appropriate HDO temperature (150-250 ºC). The reactions were carried out under strong agitation (~1,000 rpm) and a final H_2 pressure was set to 4.0 MPa when the reactor temperature approached to its setpoint. During a total of 5-hour reaction period, liquid samples were taken every hour and were filtered through a syringe filter prior to off-line analysis using an Agilent GC-MS 7890A-5975 equipped with a 30 m HP-5 column.

4.3 Results and Discussion

4.2.6   Morphology and Textural Properties of Meso-ZSM-5

As shown in Figure 1a, the XRD patterns of samples obtained from the solid-state crystallization method (Meso-ZSM-5) and traditional hydrothermal method (ZSM-5) are identical. Both match the characteristic diffraction pattern of MFI type crystal, indicating the same ZSM-5 crystalline framework for zeolites received from both our solid crystallization and traditional hydrothermal methods. As depicted in Figure 4-1b, the NH_3 TCD signal profiles of Meso-ZSM-5 and microporous ZSM-5 are almost identical, with three separated desorption peaks centered at ca. 165 °C, ca. 330 °C, and 720 °C, which correspond to the medium, strong, and ultra-strong acid sites of zeolites, respectively. This confirms that with the same Si/Al ratio, Meso-ZSM-5 zeolites synthesized by solid

nanogel crystallization also show similar acid strength, both on total acidity and for individual acid types, with traditional ZSM-5 counterparts.
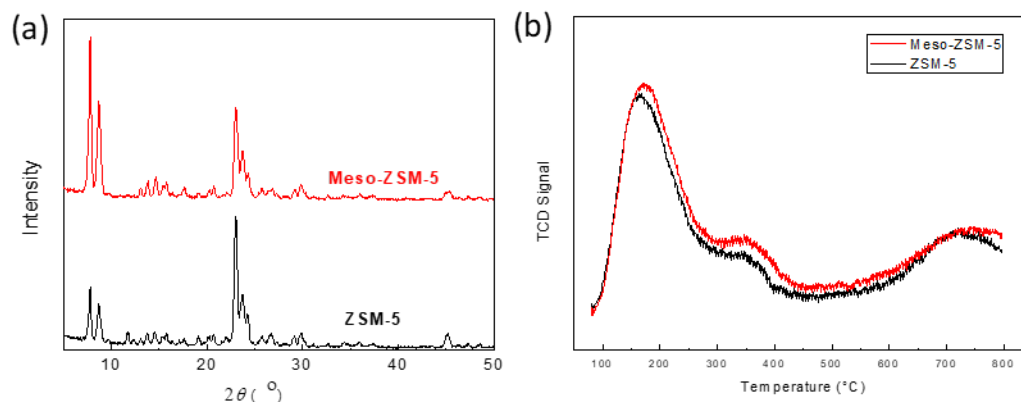
Figure 4-1: (a) XRD patterns and (b) NH$_3$-TPD results of Meso-ZSM-5 and ZSM-5 zeolites.

Although having similar crystal and acidity, the morphology of zeolites obtained by solid crystallization of aluminosilicate nanogels is quite different from those synthesized through traditional hydrothermal approaches. Rather than the elongated, hexagonal plate shape of conventional microporous ZSM-5 zeolites with smooth surface and an average dimensions of ~225×500×700 nm (Figure 4-2a), Meso-ZSM-5 zeolites have rough surface and a spherical shape (~300-400 nm), attributed to the assembly and fusion of many zeolites nanocrystals of 20-30 nm into a large monolithic piece with connected inter-lattice mesoscale space, as shown in Figure 4-2b. The HRTEM image further confirms the presence of the hierarchical structure on Meso-ZSM-5. As shown in Figure 4-2c, the neighbor nanocrystals in single crystalline zeolites exhibit lattice diffraction fringes in the same orientation at edges, suggesting that these nanocrystals have been grown and merged into a single, large monolithic crystal rather than randomly packed nanocrystal aggregates. The integration of those nanocrystals of 20-30 nm is

further endorsed by the selected area electron diffraction (SAED) pattern (inset of Figure

4-2c). Intracrystal mesopores can also be clearly seen in Figure 4-2c, contributing to the

free space created by the stacking of jointed nanocrystal units into a monolithic large

piece crystal.
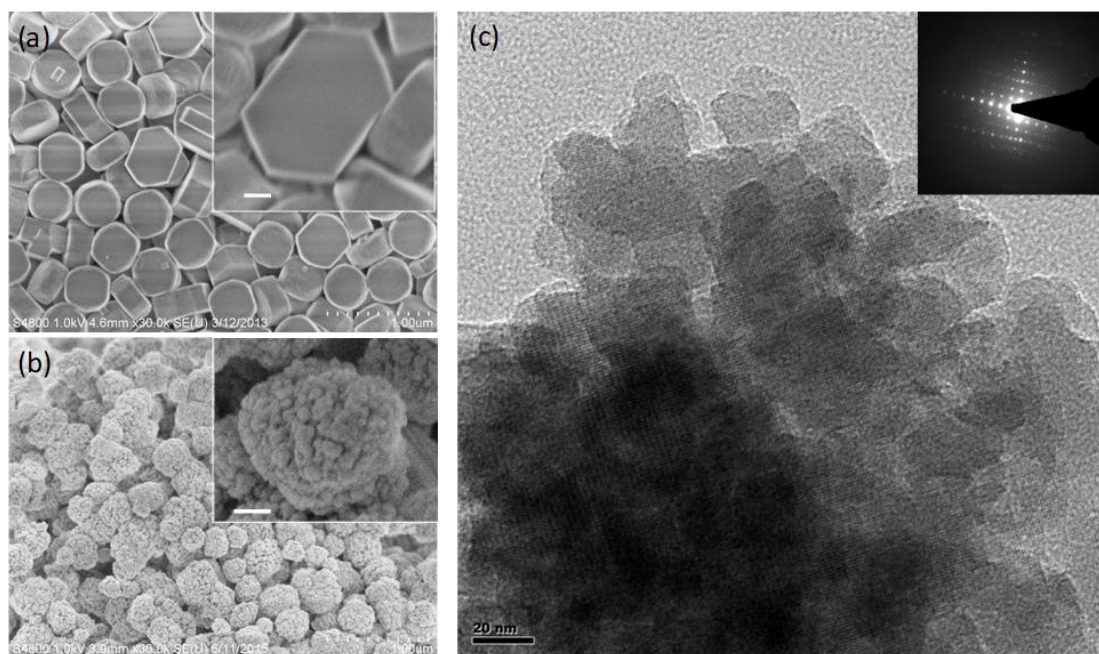
Figure 4-2: (a-b) SEM images of conventional ZSM-5 (a) and Meso-ZSM-5 (b) zeolites; (c) HRTEM images of Meso-ZSM-5. The insets in panels (a, b) are high magnification (100K) SEM images of these zeolites and the additional scale bars there represent 100 nm. The inset in panel (c) is the corresponding electron diffraction pattern of a selected area of Meso-ZSM-5.

Their hierarchical pore structure is further confirmed through the N_2 adsorption–

desorption isotherms. As shown in Figure 4-3a, conventional microporous ZSM-5

presents a classic type I adsorption/desorption isotherm for microporous materials, which

has only one high uptake at low relative pressure (P/P0 < 0.02) and a long plateau in the

high-pressure range (0.4 < P/P0 < 0.9). On the contrary, Meso-ZSM-5 zeolites present a

combination of both type I and type IV adsorption/desorption profiles with two uptake

steps, a steep one at P/P0 < 0.02 followed by a slow one afterward, responding for micropore filling and mesopore capillary condensation, respectively. A hysteresis loop at 0.45 < P/P0 < 0.90 locations suggests the existence of hierarchical pore structure in Meso-ZSM-5 zeolites. The textural parameters (Table 4-1) further reveal that Meso-ZSM-5 has evidentially larger BET surface area (424.2 m^2/g vs 317.9 m^2/g), larger pore volume (0.28 cm^3/g vs 0.15 cm^3/g), and larger average BJH pore size (8.4 nm vs 3.0 nm) when compared to its microporous counterpart. Such increases are mostly attributed to the introduction of mesopores in Meso-ZSM-5. Although BET method underestimates the contribution of micropores to the total surface area of zeolites, its accuracy on mesoporous structure measurement at least confirms the availability of many mesopores in our Meso-ZSM-5 zeolite crystals and their contribution to the increase of the apparent surface area on accessible to probe molecules (i.e, N_2) BET method calculates. The extracted surface area and pore volume information from N_2 adsorption–desorption isotherms are provided here for general reference purpose, considering its wide adoption by zeolite community even today due to a historical reason and in case textural property measurement comparisons are needed with other research work. Nevertheless, even although the presence of mesopores reduces the surface area contributed by micropores if those mesoscale space was occupied by zeolite crystal, their existing provides still more accessible surface area: not only the new surface area contributed by mesopores, but also more accessible surface from micropores inside zeolite framework.
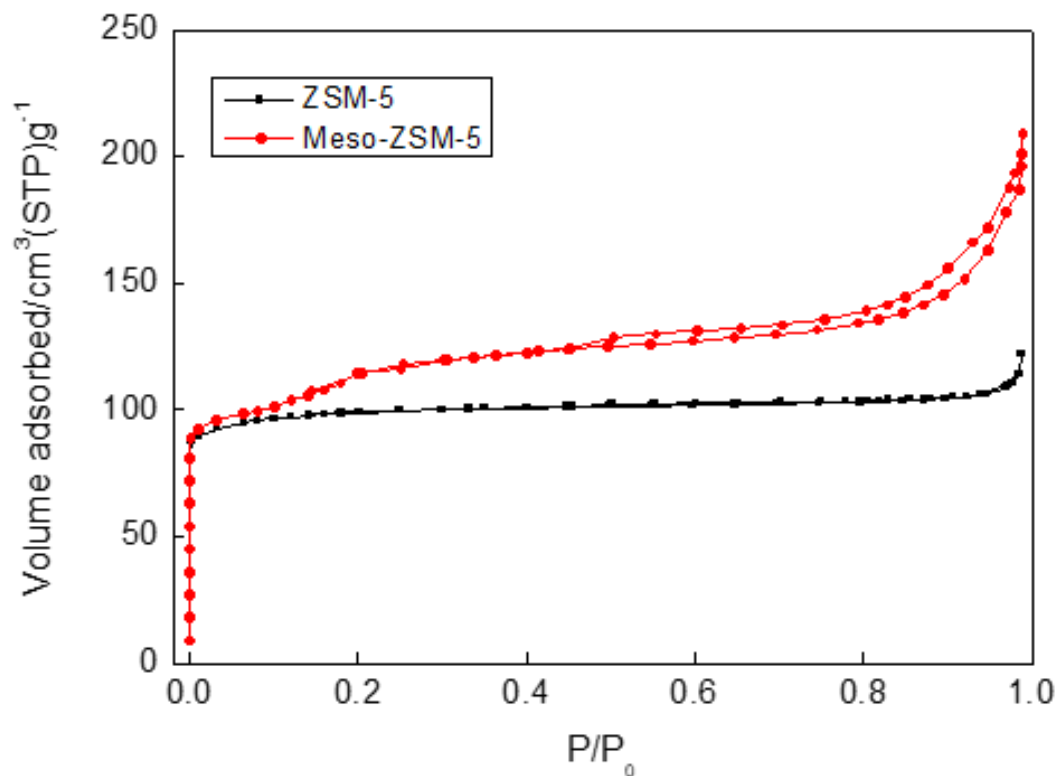
Figure 4-3: N$_2$ sorption isotherm of Meso-ZSM-5 and conventional ZSM-5.

Table 4-1: Textural Properties of Meso-ZSM-5 and Conventional ZSM-5

Sample	S$_{BET}$ [m²/g]	V$_{total}$[cm³/g][a]	Pore Size [nm][b]	Pd Dispersion (%)	Active Particle Diameter (nm)
Meso-ZSM-5	424.2	0.28	8.4	73.6	1.54
ZSM-5	317.9	0.15	3.0	34.2	3.32

[a] Single point total pore volume at P/P0 = 0.98. [b] BJH adsorption average pore size.

4.2.7   Morphology and Textural Properties of Palladium/Meso-ZSM-5 Catalyst

The unique hierarchical pore structure of Meso-ZSM-5 also affects the size and

dispersion of metal particles over zeolite support. After converting zeolites to H-type, 0.5

wt.% Pd was loaded on both types of zeolites by conventional incipient wetness

impregnation to form Pd/ZSM-5 and Pd/Meso-ZSM-5 catalysts. For Pd/Meso-ZSM-5

catalyst, palladium nanoparticles of an average of 3 nm are uniformly dispersed on the surface of zeolite crystal framework (Figure 4-4). The BET surface area of Pd/ZSM-5 catalyst still has 378.3 m^2/g after 0.5wt.% palladium loading, suggesting no large aggregates of palladium particles. In contrast, the BET surface area of Pd/ZSM-5 drops to 233.6 m^2/g due to the occurrence of obvious metal aggregation and micropore blocking issues. The palladium dispersion analysis by H_2-TPD results confirm this claim with much better palladium dispersion on Meso-ZSM-5 than that on ZSM-5 (73.6% for Pd/Meso-ZSM-5 vs 34.2% for Pd/ZSM-5, as shown in Table 4-1). Correspondingly, the calculated active particle diameter is smaller for Pd/MesoZSM-5 (1.54 nm) than Pd/ZSM-5 (3.32 nm), as shown in Table 4-1. Although the palladium particle size calculated by H_2-TPD measurement is much smaller than that in TEM images, both results confirm that the availability of mesoporous structure helps disperse palladium nanoparticles better over Meso-ZSM-5 support than what on ZSM-5 so that smaller average particle size is achieved in Pd/Meso-ZSM-5 catalyst.
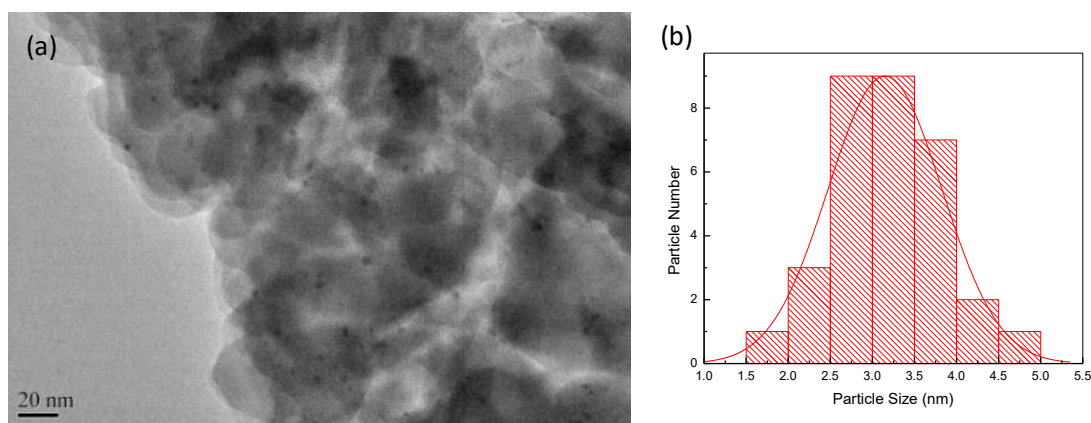

Figure 4-4: (a) HRTEM image and (b) Pd particles size distribution profile of Pd/Meso-ZSM-5 catalyst.

The H_2-TPR signals of both catalysts are shown in Figure 4-5. As in H_2-TPR, a positive peak means hydrogen consumption while a negative peak is tied with the occurrence of hydrogen desorption from catalyst surface. For palladium catalysts, negative H_2-TPR peaks could come from two processes: one is associated with H_2 release from the decomposition of palladium hydrides near 105 °C and the other is contributed by the desorption of spillover hydrogen on the support material in which that desorption temperature is around 200 °C 29. As shown in Figure 4-5, the major negative peak for Pd/Meso-ZSM-5 catalyst is around 125 °C while the major negative peak for Pd/ZSM-5 catalyst is around 220°C, both shifts 20 °C from the two characteristic H_2 desorption peak positions from the literature. Considering H_2-TPR procedure and/or instrument difference, our results suggest that the pronounced H_2 desorption peak on the H_2-TPR curve of Pd/Meso-ZSM-5 is attributed to the decomposition of palladium hydride, though a minor negative peak is also shown around 220 °C due to the spillover hydrogen. In contrast, the major H_2 release signal for Pd/ZSM-5 comes from the spillover hydrogen over microporous zeolite support. Consider there is more accessible surface area on Meso-ZSM-5 than what on microporous ZSM-5, we can further claim that most surface area of catalyst support in Pd/Meso-ZSM-5 is covered by palladium particles than what in Pd/ZSM-5. In another word, the ZSM-5 support of Pd/ZSM-5 catalyst has more exposed surface (i.e., uncovered by palladium particles) to allow significant hydrogen spillover effect. With the same Pd impregnation dosage, this means averagely smaller size and better dispersion for palladium particles over Meso-ZSM-5 than what on microporous ZSM-5. More palladium surface is accessible to H_2 probe molecules to form palladium hydrides (and release H_2 during later TPR test) (Gomez-Quero, S., *et al.* 2008),

rather than spillover on the support surface. Similar findings are also reflected in the

chemisorption analysis results on palladium particle size and dispersion (Table 4-1). A

broad positive peak ranging from 300 ºC to 400 ºC appears in both H_2-TPR curves. This

is attributed to the reduction of palladium oxides that interact strongly with some specific

acidic sites of ZSM-5 support. Protons in zeolite crystals enhance the chemical anchoring

of palladium species, making them more difficult to get reduced (Sachtler, W. M. H. and

A. Y. U. Stakneev, 1992). With similar acidity profiles for Meso-ZSM-5 and

microporous ZSM-5 support (proved by NH_3-TPD results shown in Figure 4-1b), the

reduction temperature position of this positive peak is unchanged for both zeolite

supports, implying their similar interaction strength with palladium oxides in certain

acidic sites. However, the better-defined peak shape and greater peak area for Pd/Meso-

ZSM-5 catalyst again suggest more Pd2+ ions are stabilized there on Meso-ZSM-5.

Additional broad positive peak centered at 500 ºC is also found on the H_2-TPR curve of

Pd/Meso-ZSM-5 catalyst, which is not shown for Pd/ZSM-5 catalyst. This indicates that

chemical anchoring of palladium clusters occurs on acidic sites of various acidic sites of

Meso-ZSM-5. Considering two zeolite supports (i.e., ZSM-5 and Meso-ZSM-5) have the

same acidity profile but different porous structure, it is reasonable to attribute such

difference to the accessibility of those acidic sites within the hierarchical porous structure

of Meso-ZSM-5. The different porous structures between Meso-ZSM-5 and microporous

ZSM-5 results in binding diversity of palladium species on them, which could further

cause various catalytic behaviors.
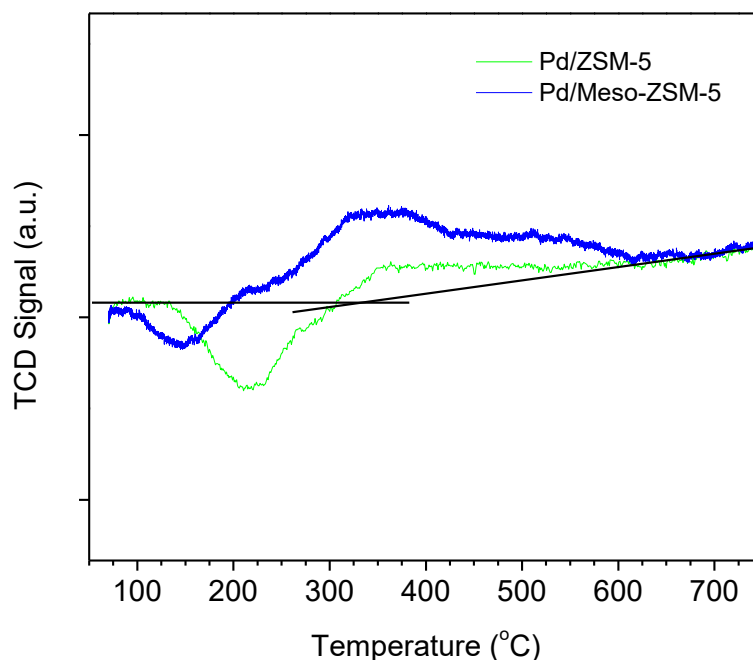
Figure 4-5: H_2-TPR profile of Pd/Meso-ZSM-5 and Pd/ZSM-5 catalysts

4.2.8   Evaluation Guaiacol Hydrodeoxygenation Performance

Most studies on guaiacol HDO were conducted at high temperature and high H_2

pressure conditions to achieve reasonable conversion (Sun, J., *et al.* 2014; Zhao, H. Y., *et*

al. 2011; Olcese, R. N., *et al.* 2012; Zhao, C. and J. Lercher, 2012; Zhu, X., *et al.* 2011).

However, relatively low reaction temperature and H_2 pressure are often preferred in

industrial practice to compromise overall requirements among HDO efficiency, overall

energy consumption, and coking formation issues. Therefore, our comparison of guaiacol

HDO performance between Pd/Meso-ZSM-5 and Pd/ZSM-5 was made at relatively low

temperature (150-250 °C) with a H_2 pressure of 4 MPa.

The conversion of guaiacol and its HDO product distribution strongly depend on

the reaction temperature. As shown in Figure 5a, both catalysts are very inactive in

guaiacol HDO reactions at 150°C. For Pd/ZSM-5, less than 5 % guaiacol is converted

after the 5-hour reaction period. Despite having more accessible active sites and

improved intra-particle diffusion, even Pd/Meso-ZSM-5 gets only 19% guaiacol reacted.

The main products of guaiacol HDO at this temperature include monoxygenated

compounds such as cyclohexanone (~11% of the total test sample, as shown in Figure 4-

6b). This suggests that hydrogenation of guaiacol could occur, though not effective, over

ZSM-5 supported palladium catalyst surface at 150 °C. Under such a low HDO

temperature, the benzene ring saturation dominates all involved reactions while

deoxygenation is largely limited to the removal of methoxy groups on guaiacol molecular

structure so that more than 50% of all HDO products is cyclohexanone. Oxygenate-free

products are very low, suggesting deep deoxygenation reactions (e.g., removal of the

phenol hydroxyl group) are far from competitive with hydrogenation of benzene ring at

this low temperature.
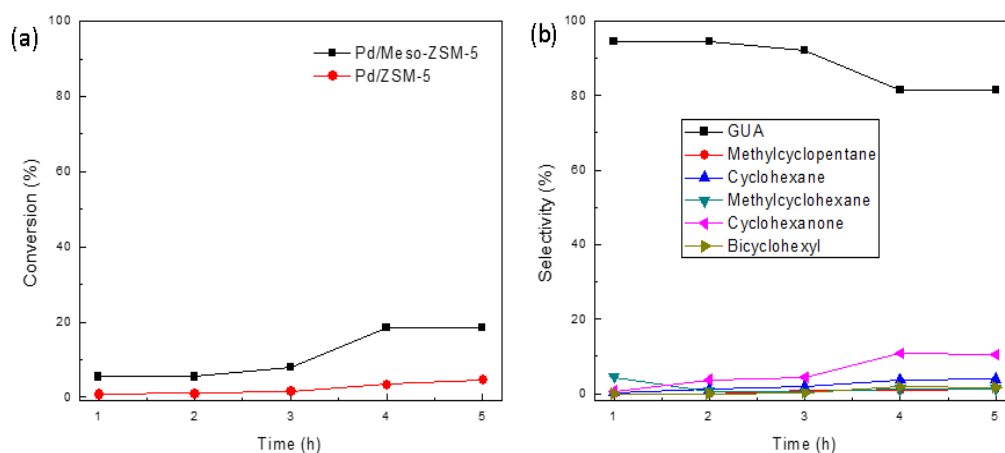
Figure 4-6: (a) Guaiacol conversion and (b) product distributions over Pd/Meso-ZSM-5 and Pd/ZSM-5 at a hydrodeoxygenation temperature of 150°C

Elevating the reaction temperature to 200 °C significantly improve the activity and selectivity of both catalysts in guaiacol HDO reactions (Figures 4-7a, 4-7b, and 4-8). With the HDO reactions continue, the conversion of guaiacol climbs rapidly to ~84% over Pd/Meso-ZSM-5 and ~36 % over Pd/ZSM-5 within the 5-hour reaction time (Figure 4-7b). Complete deoxygenation and hydrogenation become very efficient with main HDO products saturated, oxygenate-free cyclohydrocarbons such as methylcyclohexane, cyclohexane, and methylcyclopentane (Figures 4-7a & 4-8c), whose percentage in all products accumulates quickly with reactions ongoing (Figure 4-7c). Compared to what occurred over Pd/ZSM-5 catalyst, the guaiacol HDO degree on mesoporous zeolites supported one (i.e., Pd/Meso-ZSM-5) shows a 2.5 fold increase after the 5-hour reaction period and the oxygen-free and ring-saturated products reach 72% of the total test samples (Figure 4-8). In contrast, only ~31% of similar products are received over Pd/ZSM-5 catalyst. The incomplete guaiacol conversion allows detection of intermediate HDO products. Some monoxygenate compounds such as cyclohexanone are found in the products and their presence starts from the beginning of the HDO reactions over Pd/Meso-ZSM-5 catalyst, with a total partition slowly accumulated from ~4.8% to 11.3% of all compounds in the test samples within the 5-hour reaction period (Figure 4-7c). For Pd/ZSM-5 catalyst, such percentage is ~5.9% after the 5-hour HDO reaction period (Figure 4-6c). Based on the position of remaining oxygen molecules on these partially deoxygenated intermediates, the scission of aromatic-methoxy bonds seems much easier than the breakdown of the phenol hydroxyl groups. A small quantity of aromatics (e.g., cyclohexyl benzene) is also detected in HDO product and their percentage steadily rises with continuous consumption of guaiacol (Figure 4-7c). Despite the similar kinetic

profile, the partition of these unsaturated, oxygenate-free hydrocarbons (i.e., aromatics) always falls behind that of monoxygenate compounds 5% or more in the test samples. This further supports the suggested HDO routes over palladium catalyst -- hydrogenation has a higher priority to saturate the benzene ring so that benzylation reactions only occur when enough monoxygenate HDO intermediates accumulate in the reaction system. However, the competition between hydrodeoxygenation and hydrogenation alone (suturing the benzene ring) always exists, depending on the reaction temperature. As hydrogenation favors low temperature operation as long as having enough dissociated hydrogen while deoxygenation requires much higher reaction temperature to break down C-OH bonds of phenols, further increase of the HDO temperature could shift this reaction preference to deoxygenation dominated routes (Figure 4-9a).
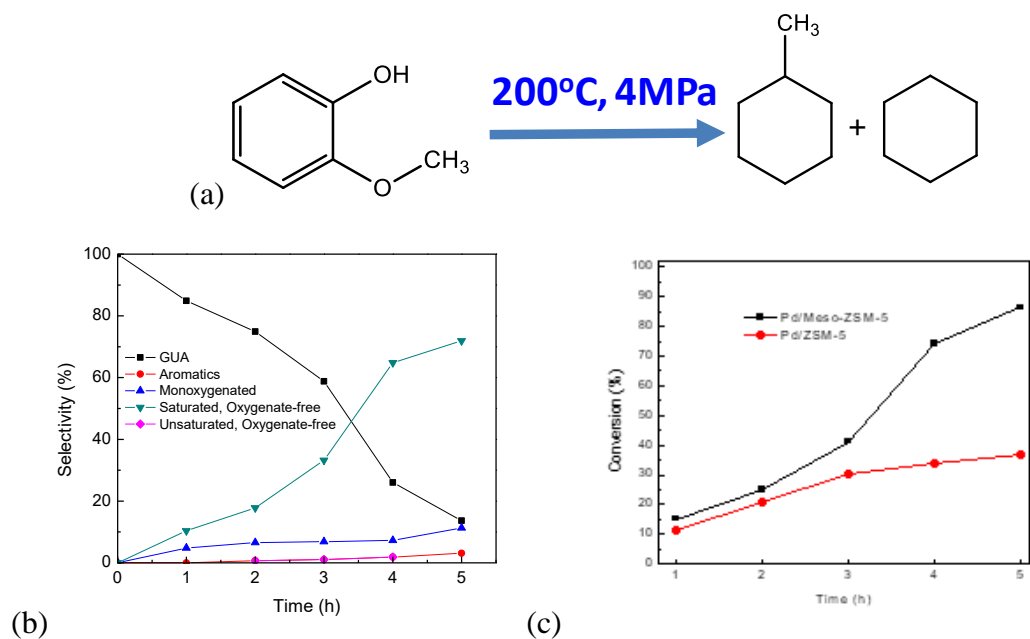
Figure 4-7: (a) GUA HDO reaction routes, (b) GUA conversion, and (c) kinetics 5-hour HDO reaction of GUA at 200C over Pd/Meso-ZSM-5 and Pd/ZSM-5 catalysts
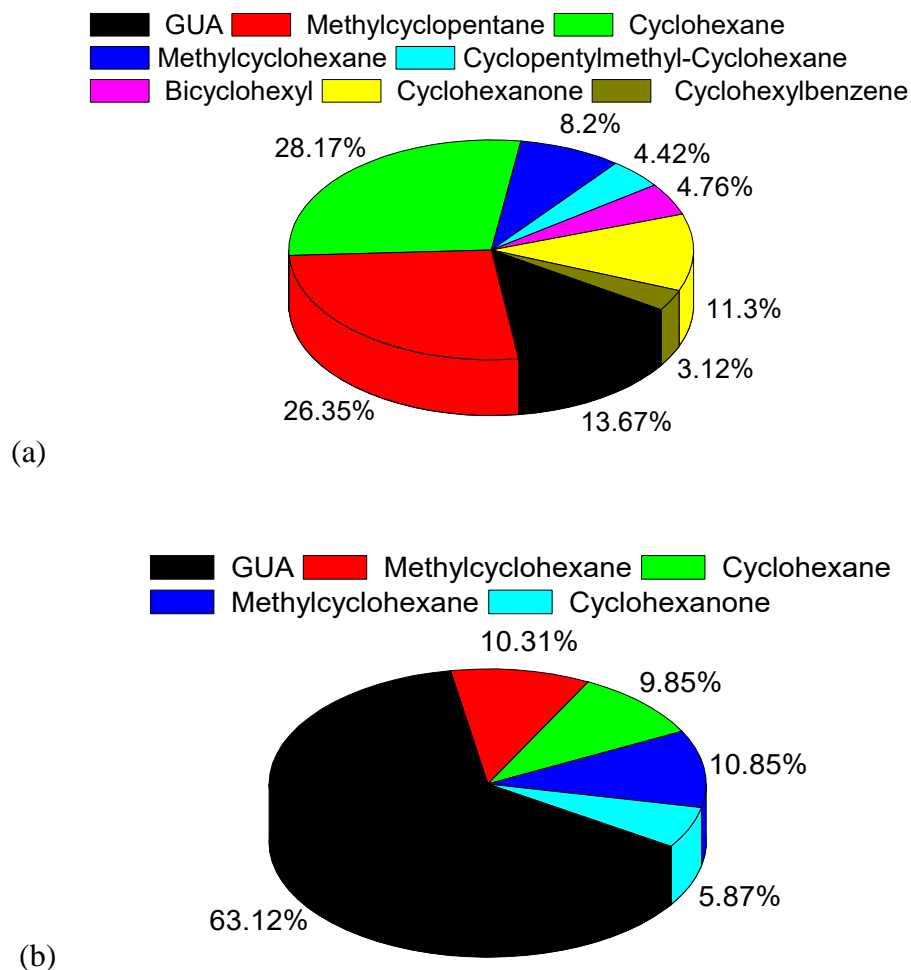
Figure 4-8: The products distribution after 5-hour HDO reaction of GUA at 200 °C over Pd/Meso-ZSM-5 (a) and Pd/ZSM-5 (b) catalysts. Note: most "unsaturated, oxygenate-free" products overlay with "aromatics" except the former include olefins.

To verify this hypothesis, we further elevated the reaction temperature to 250°C. At this temperature, notwithstanding, the guaiacol conversion gets further improved. Within only 3 hours, guaiacol is completely reacted over Pd/Meso-ZSM-5 and this takes only slightly longer for Pd/ZSM-5 (i.e., 4 hours), as shown in Figure 4-9b. More important, the HDO product composition is significantly changed. Despite its more diverse products, only oxygen-free compounds were detected, indicating the effective deoxygenation ability of both catalysts at 250 °C. Besides deoxygenation, the high

temperature also triggers other endothermic reactions such as methanization of aromatic rings. Unlike at 200 °C that oxygen-free and ring-saturated products dominate, these compounds account only 3% of all products over Pd/Meso-ZSM-5 and 6% over Pd/ZSM-5 at 250 °C (Figure 4-10). In contrast, the percentage of heavy polymethylated aromatic products, such as methylated benzene (i.e., toluene, dimethyl benzene, ethyl benzene, 1-methyl, 2-ethyl benzene, and tri-methyl benzene) and methylated cyclohexene (i.e., methylcyclohexene and dimethylcyclohexene), increases rapidly with HDO ongoing (Figure 4-9c) and eventually contribute over 94% of all products for both catalysts after 5 hours. These results together suggest that deoxygenation overturns hydrogenation as the dominating process at 250 °C. Similar phenomena have also been found in guaiacol HDO process over Co and Ni catalysts (Tran, N. T. *et al*. 2016; Luo, Y. R., 2007). This is reasonable as exothermic reactions such as benzene ring saturation become unfavorable at elevated reaction temperature when compared with endothermic reactions like hydrogenation. Further hydrogenation of benzene rings after the removal of methoxy group therefore becomes less competitive than deoxygenation. Deep deoxygenation on the hydroxyl group of phenols also activates α and β hydrocarbon groups on the benzyl ring, triggering polyalkylation reactions at elevated temperature. Such reaction preference shift (i.e., from hydrogenation domination to deoxygenation domination) results in significant amount of heavy polymethylated aromatics in the HDO product of guaiacol at 250 °C.

(a)
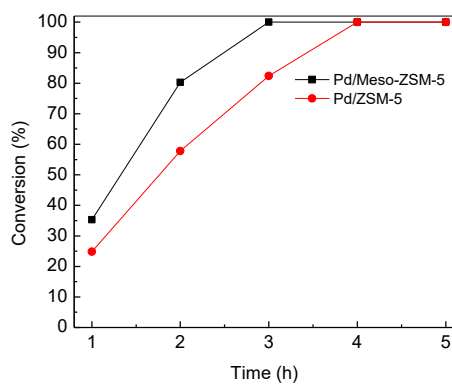
(b)
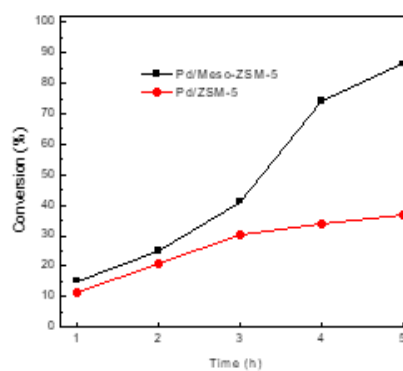
(c)

Figure 4-9: (a) GUA HDO reaction routes, (b) GUA conversion, and (c) kinetics in 5-hour HDO reaction of GUA at 250 °C over Pd/Meso-ZSM-5 and Pd/ZSM-5 catalysts
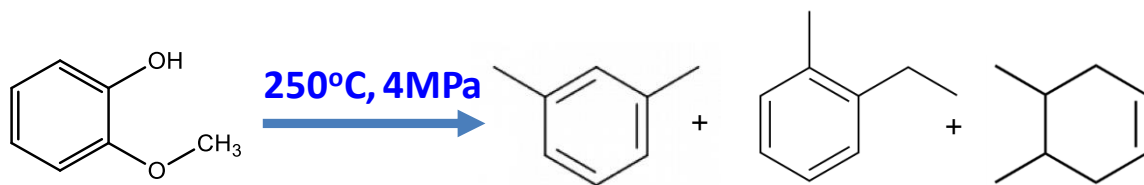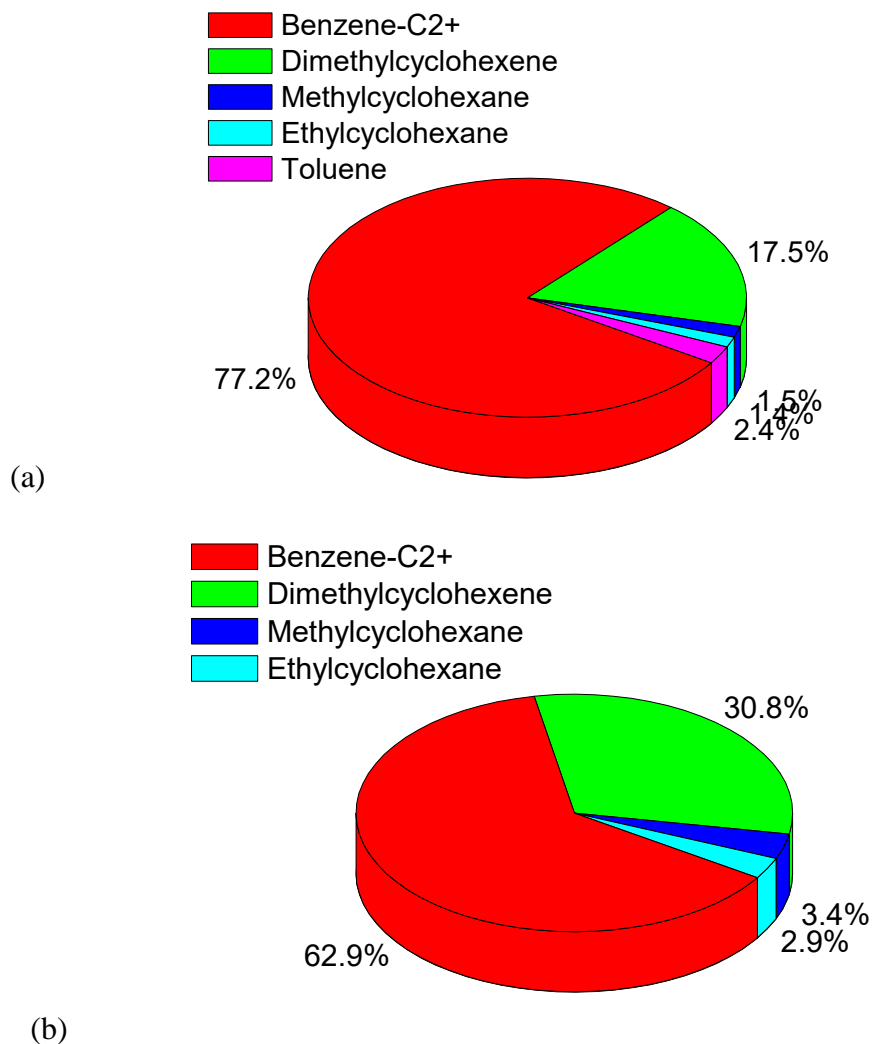
Figure 4-10: Products distribution after 5h HDO reaction of GUA at 250 °C over Pd/Meso-ZSM-5 (a) and Pd/ZSM-5 (b) catalyst. Note: most "unsaturated, oxygenate-free" products overlay with "aromatics" except the former include olefins

Although the high HDO temperature helps improve the guaiacol conversion and deoxygenation degree, unsaturated, polymethylated aromatics are formed, which, if presenting a large quantity within molecule transport pathways inside catalyst, would quickly accumulate on its active sites as coke and deactivate the catalyst. For our case, after the 5-hour HDO reaction, the used Pd/Meso-ZSM-5 catalyst still retained its original gray color while the used Pd/ZSM-5 catalyst turned to brown (Figures 4-11a &

4-11b), indicating their different coking situations. The amount of coke on both catalysts was further quantified with TGA. As shown in Figure 4-11c, besides the early 4% mass loss contributed by water adsorbed on catalyst samples, additional ~8% mass loss occurs over Pt/Meso-ZSM-5 catalyst owing to the decomposition of coke deposited on catalyst during the 5-hour HDO reaction. For Pd/ZSM-5 catalyst, the formed coke contributes a mass loss of 12% (or a 50% increase) in TGA measurement. Such coking formation difference is believed the result of additional mesopores and multiple-scale reactant/product diffusion highways created in Pd/Meso-ZSM-5 catalyst, which largely mitigate the formation of rich hydrocarbon pool that is often seen in catalysts with only microporous structure such as Pd/ZSM-5 in this work. Besides molecule transport promotion within catalyst, the unique hierarchically porous structure of Meso-ZSM-5 also makes palladium particles better distributed over the zeolite support surface to gain more accessible activate sites to slow down their deactivation. All these merits benefit the better guaiacol HDO performance over Pd/Meso-ZSM-5 than what on Pd/ZSM-5 at relatively low temperature (150-250 °C).
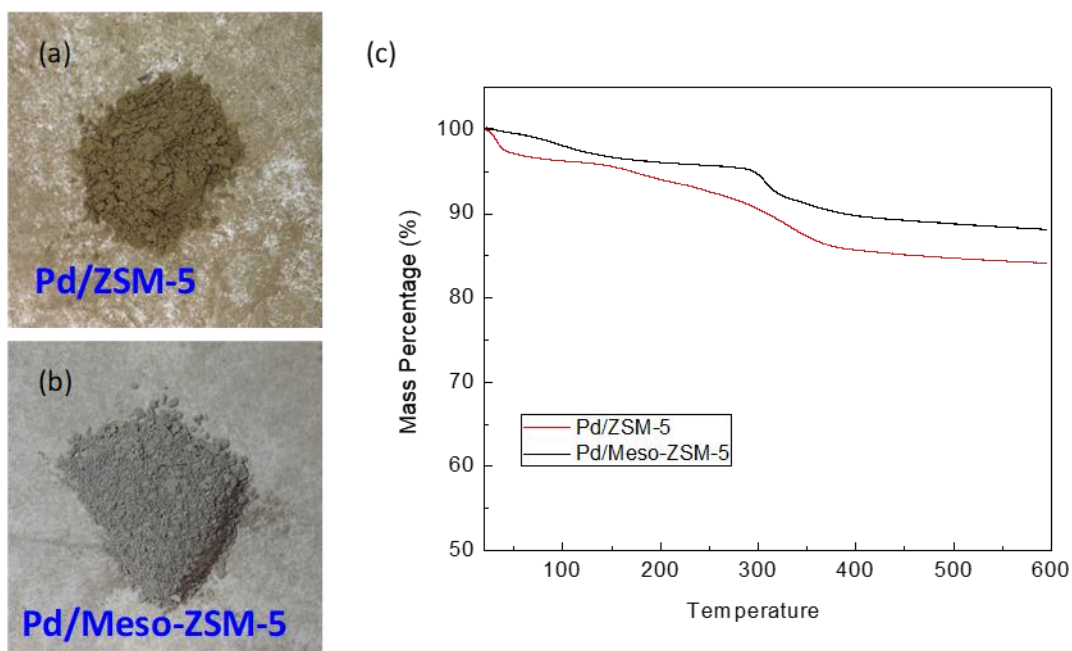
Figure 4-11: Optical photos of Pd/Meso-ZSM-5 (a) and Pd/ZSM-5 (b) after 5-hour GUA HDO reaction at 200 °C; (c) TGA results of coking evaluation on these catalysts

4.3 Conclusions

In summary, new mesoporous zeolites ZSM-5 (Meso-ZSM-5) is successfully produced from aluminosilicate nanogels under solid-state crystallization conditions without hydrothermal synthesis and assembly process. These ZSM-5 zeolites have unique hierarchical pore geometry created by joining and stacking of many zeolite nanocrystals at adjacent crystalline edges. A hydrodeoxygenation process was used to effectively upgrade the important bio-oil compound, guaiacol. For this process, palladium was loaded and well dispersed on Meso-ZSM-5 to form Pd/Meso-ZSM-5 catalyst. Attributed to fast diffusion and easy accessibility for reactants and/or products, the formed catalyst shows superior catalytic conversion and anti-coking performance at various temperature conditions when compared with catalyst supported on conventional microporous ZSM-5

zeolites. These results demonstrate the great potential of Pd/Meso-ZSM-5 catalyst in bio-oil upgrading and other hydrotreating reactions involving bulky molecules.

CHAPTER 5

CONCLUSIONS AND FUTURE WORK

5.1   Conclusions

The acidity and pore structure of different zeolites effect on lignin depolymerization in supercritical ethanol has been examined. Those zeolites include that with similar pore size, HBeta and HZSM-5, and those with similar acidity, HBeta and HY. Further examination into lignin depolymerization included evaluation of mesopores and micropores of HZSM-5 and HY zeolites. HBeta and HY, due to their strong acidity, were found to break down the lignin structure to produce phenols, while HZSM-5 having less acidity broke down the ether bonds. The hierarchically porous structure of the zeolites allowed them to utilize the acidic sites to break down bulky molecules. With bulky lignin, diffusion becomes less severe and acidity becomes dominant in selectivity of lignin depolymerization products. This allows tailoring of the design of zeolites which decreases plant material waste and promotes the conversion of aromatic units into high-value chemicals and fuels.

Palladium loaded on new ZSM-5 zeolites with unique hierarchically porous structure (Meso-ZSM-5) synthesized by solid crystallization from aluminosilicate nanogels. Such mesoporous zeolites (Pd/Meso-ZSM-5) showed well dispersion on zeolite nanocrystals. Attributed to fast diffusion and easy accessibility for reactants and/or products, the formed catalyst shows superior catalytic conversion and anti-coking

performance at various temperature conditions when compared with catalyst supported on conventional microporous ZSM-5 zeolites when used for lignin depolymerization product upgrade by hydrodeoxygenation process. Ring saturated hydrocarbons are largely produced at 200 °C when hydrogenation dominates while alkylated aromatics become major HDO products as deoxygenation becomes favorable at 250 °C. These results demonstrate the great potential of Pd/Meso-ZSM-5 catalyst in bio-oil upgrading and other hydrotreating reactions involving bulky molecules.

5.2   Future Work

The findings of this project on the roles of solid acidity and porous structures of zeolites on lignin depolymerization provide important guidelines on the selection and design of zeolites to further facilitate lignin depolymerization or other cracking processes. Only Kraft lignin was used in the studies in this project. Other types of lignin such as organosolv or alkaline lignin are also worthy of investigation to find out the validity of the revealed relationships between acidity and porous structure of zeolites to the depolymerization performance, particular the yields of phenols with single benzene ring and the intermediate products such as 1,2-Dimethoxy-4-(1-methoxyethenyl)benzene. Model molecules mimicking a variety of bonds (e.g., the C-O-C and C-C linkages) within the molecular structure of lignin could be used to simplify the analysis and correlation on how zeolites with particular acidity and porous structures perform to cleave these bonds. The possibility of using the mixture of zeolites of different types to tailor the overall acidity, and porous structures is also worth to explore on the contribution to effective lignin depolymerization. Such choices of zeolites catalysts or other zeolites with unique porous structures such as HZSM-5 with fin-like mesopores used in this dissertation

project is also worthy of exploration on other biomass conversion processes such as catalytical pyrolysis and hydrolysis in sub-and super-critical water conditions.

The new mesoporous zeolites used in this project were loaded with palladium and their hydrodeoxygenation performance was examined. Other hydrotreating catalyst metals, including previous metals such as Pt and Ru as well as transition metals such as Ni, Co-Mo, and Ni-Mo are also worthy of investigation on their hydrodeoxygenation performance of lignin depolymerization products as well as other hydrotreating processes such as HDS and HDN. Various hydrogen pressure and reaction temperature conditions should be examined. Other heating or energy supply schemes such as microwave heating and electrochemical activation of hydrogenation are also worthy of exploration.

Zeolites are heavily involved in lignin depolymerization (with a catalyst-to-reactant ratio often larger than 1:1) and a double-template method was used in this project to synthesize zeolites with fin-like mesoporous structure using traditional hydrothermal synthesis process. Such zeolite production requires the use of a large quantity of solvent (e.g., water and ethanol) which takes 70-80% volume of the high-pressure vessels used in hydrothermal synthesis while collects only 10-20% solid product. This not only increases the equipment and operation cost and energy consumption during such high-pressure synthesis systems, but also leaves a significant amount of toxic liquid waste containing alkali, silicates, and aluminates, which adds more cost on post-synthesis separation and additional risk of human helath and penalty on environmental pollution. These issues become more serious in biomass-based renewable energy processes with their significantly high quantity demand of zeolites, which could largely offset the potential benefits of these bioenergy routes considering the new pollution concerns or negative

impact to environment initiated by the involved zeolite industry. In the future, new, low-cost, and environmental benign strategies sould be explored in hierarchically porous zeolite synthesis so that the overal lignin utilization cost can be significantly reduced to some comparable levels to make it competitive with the current fossil fuel product price.

BIBLIOGRAPHY

Abdullah, N., et al. "Characterization of Banana (Musa spp.) Plantation Wastes as a Potential Renewable Energy Source," *AIP Conference Proceedings*, vol. 1528, no. 1, May 2013 pp. 325–330.

ArneStahl, A., et al. "Formic-Acid-Induced Depolymerization of Oxidized Lignin to Aromatics," *Nature*, vol. 515, no. 7526, Nov. 2014, pp. 249–252.

Baglio, V. et al., "Zeolite-Based Composite Membranes for High Temperature Direct Methanol Fuel Cells," *Journal of Applied Electrochemistry*, vol. 35, no. 2, Feb. 2005, pp. 207–212.

Bernier, P. and D. Paré, "Using Ecosystem CO_2 Measurements to Estimate the Timing and Magnitude of Greenhouse Gas Mitigation Potential of Forest Bioenergy," *GCB Bioenergy*, vol. 5, no. 1, Jan. 2013 pp. 67–72.

Bhardwaj, D., "Hydrothermal Synthesis and Characterization of Zeolite: Effect of Crystallization Temperature." *Journal of Chemical Research*, vol. 3, no. 9, Sep. 2013, pp. 1–4.

Bingjun, Xu, et al. "Enhanced Stability of HZSM-5 Supported Ga_2O_3 Catalyst in Propane Dehydrogenation by Dealumination," *Catalysis Letters*, vol. 119, no. 3/4, Dec. 2007, pp. 283–288.

Bjelic, A., et al. "Catalytic Hydrogenation, Hydrodeoxygenation, and Hydrocracking Processes of a Lignin Monomer Model Compound Eugenol over Magnetic Ru/C–Fe_2O_3 and Mechanistic Reaction Microkinetics." *Catalysts*, vol. 8, issue 10, 2018, pp. 425-444.

Bjelic, A., et al. "Hydrogenation and Hydrodeoxygenation of Aromatic Lignin Monomers over Cu/C, Ni/C, Pd/C, Pt/C, Rh/C and Ru/C Catalysts: Mechanisms, Reaction Micro-Kinetic modelling and Quantitative Structure-Activity Relationships." *Chemical Engineering Journal*, vol. 359, 2019, pp. 305-320.

Castillo-Villar, K. K. "Metaheuristic Algorithms Applied to Bioenergy Supply Chain Problems: Theory, Review, Challenges, and Future," *Energies*, vol. 7, no. 11, Nov. 2014, pp. 7640–7672.

Chai, L., et al. "Depolymerization and Decolorization of Kraft Lignin by Bacterium Comamonas sp. B-9," *Applied Microbiology and Biotechnology*, vol. 98, no. 4, Feb. 2014, pp. 1907–1912.

Chao, Jin, et al. "Anionic Emulsion-Mediated Synthesis of Zeolite Beta," *Intermational Journal of Modern Physics B: Condensed Matter Physics, Statistical Physics, and Applied Physics*, vol. 24, no. 15/16, Jun. 2010. pp. 3236–3241.

Chen, Jiao, et al. "Catalytic Fast Pyrolysis of Alcell Lignin with Nano-NiO," *BioResources*, vol. 11, no. 1, Feb. 2016, pp. 663–673.

Choi, M., et al. "Amphiphilic Organosilane-Directed Synthesis of Crystalline Zeolite with Tunable Mesoporosity." *Nature Materials,* vol. 5, 2006, pp. 718–723.

Dautzenberg, G., et al. "Bio Based Fuels and Fuel Additives from Lignocellulose Feedstock via the Production of Levulinic Acid and Furfural," *International Journal of Biology, Chemistry, and Physical Technology of Wood*, vol. 65, no. 4, Jun. 2011, pp. 439–451.

Deng, Z., et al. "A Hierarchical Bulky ZSM-5 Zeolite Synthesized via Glycerol-Mediated Crystallization using a Mesoporous Steam-Treated Dry Gel as the Precursor," *New Journal of Chemistry*, vol. 39, no. 10, 11 2015, pp. 7777–7780.

Ding, J., et al. "Catalytic Properties of a Hierarchical Zeolite Synthesized from a Natural Aluminosilicate Mineral without the Use of a Secondary Mesoscale Template," *ChemCatChem*, vol. 5, no. 8, Aug. 2013, pp. 2258–2269.

Diop, A., et al. "Kraft Lignin Depolymerization in an Ionic Liquid without a Catalyst," *BioResources*, vol. 10, no. 3, Jun. 2015 pp. 4933–4946.

Du, X, and E. Wu, "Porosity of Microporous Zeolites A, X and ZSM-5 Studied by Small Angle X-ray Scattering and Nitrogen Adsorption." *Journal of Physics and Chemistry of Solids,* vol. 68, issue 9, 2007, pp. 1692-1699.

Fan, L. et al. "Liquid-phase Hydrogenation of Phenol to Cyclohexanone over Supported Palladium Catalysts." *Bulletin of Chemical Reaction Engineering and Catalysis,* vol. 11, issue 3, 2016, pp. 354-362.

Gao, D., et al. "Guaiacol Hydrodeoxygenation over Platinum Catalyst: Reaction Pathways and Kinetics," *Industrial & Engineering Chemistry Research*, vol. 54, no. 43, Nov. 2015, pp. 10638–10644.

Garcia-Martinez, J. et al., "Evidence of Intracrystalline Mesostructured Porosity in Zeolites by Advanced Gas Sorption, Electron Tomography and Rotation Electron Diffraction," *ChemCatChem,* vol. 6, no. 11, Nov. 2014, pp. 3110–3115.

Gomez-Quero, S., et al. "Effect of Metal Dispersion on the Liquid-Phase Hydrodechlorination of 2,4-Dichlorophenol over Pd/Al$_2$O$_3$a." *Industrial & Engineering Chemistry Research,* vol. 47, issue 118, 2008, pp. 6841–6853.

Griffin, M. B., et al. "An Investigation into Support Cooperativity for the Deoxygenation of Guaiacol over Nanoparticle Ni and Rh$_2$P." *Catalysis Science & Technology*, vol. 7, 2017, pp. 2954-2966.

Grigor'eva, N., et al. "Oligomerization of 1-Octene on Micro-Mesoporous Zeolite Catalysts," *Petroleum Chemistry*, vol. 53, no. 6, Nov. 2013, pp. 407–411.

Grilc, M., et al. "Hydrotreatment of Solvolytically Liquefied Lignocellulosic Biomass over NiMo/Al$_2$O$_3$ Catalyst: Reaction Mechanism, Hydrodeoxygenation Kinetics and Mass Transfer Model Based on FTIR." *Biomass and Bioenergy,* vol. 63, 2014, pp. 300-312.

Guo, M. et al., "Bioethanol from Poplar Clone Imola: an Environmentally Viable Alternative to Fossil Fuel?," *Biotechnology for Biofuels*, vol. 8, no. 1, Sep. 2015 pp. 1–21.

Gyergyek, S., et al. "Magnetically Separable Ru-Based Nano-Catalyst for the Hydrogenation/Hydro-Deoxygenation of Lignin-Derived Platform Chemicals." *Materials Research Letters,* vol. 6, 2018, pp. 426-431.

Hanaoka, Toshiaki, et al. "Effects of Catalyst Preparation on Hydrocarbon Product Distribution in Hydrocracking of the Fischer-Tropsch Product with Low Pt-Loaded Catalysts," *Catalysts* 2073-4344, vol. 5, no. 4, Dec. 2015, pp. 1983–2000.

Hernando, H., et al. "Assessing Biomass Catalytic Pyrolysis in Terms of Deoxygenation Pathways and Energy Yields for the Efficient Production of Advanced Biofuels." *Catalysis Science & Technology*, vol. 6, 2016, pp. 2829-2843.

Hong, D. Y., et al. "Hydrodeoxygenation and Coupling of Aqueous Phenolics over Bifunctional Zeolite-Supported Metal Catalysts." *Chemical Communications,* vol. 46, 2010, pp. 1038-1040.

Hosseini, M., et al. "Ultrasound-Assisted Dealumination of Zeolite Y," *Journal of Chemical Sciences*, vol. 127, no. 1, Jan. 2015, pp. 25–31.

Hughes, S. R. et al., "Sustainable Conversion of Coffee and Other Crop Wastes to Biofuels and Bioproducts using Coupled Biochemical and Thermochemical Processes in a Multi-Stage Biorefinery Concept," *Applied Microbiology and Biotechnology.*, vol. 98, no. 20, Oct. 2014. pp. 8413–8431.

Hunns, J. A. et al. "Hierarchical Mesoporous Pd/ZSM-5 for the Selective Catalytic Hydrodeoxygenation of *m*-cresol to Methylcyclohexane." *Catalysis Science & Technology,* vol. 6, 2016, pp. 2560-2564.

Infantes-Molina, A. et al. "Nickel and Cobalt Phosphides as Effective Catalysts for Oxygen Removal of Dibenzofuran: Role of Contact Time, Hydrogen Pressure and Hydrogen/Feed Molar Ratio." *Catalysis Science & Technology,* vol. 5, 2015, pp. 3403-3415.

Jo, C., et al. "MFI Zeolite Nanosponges Possessing Uniform Mesopores Generated by Bulk Crystal Seeding in the Hierarchical Surfactant-Directed Synthesis," *Chemical Communications*, vol. 50, no. 32, Mar. 2014, pp. 4175–4177.

Kordouli, E., et al. "HDO Activity of Carbon-Supported Rh, Ni and Mo-Ni Catalysts." *Molecular Catalysis*, vol. 441, 2017, pp. 209-220.

Lai, Q., et al. "Mo-Pt Overlayers as Efficient Catalysts for Hydrodeoxygenation of Guaiacol and Anisole." *Catalysis Science & Technology,* vol. 7, 2017, pp. 3220-3233.

Lou, R., et al. "Pyrolytic Products from Rice Straw and Enzymatic/Mild Acidolysis Lignin (EMAL)," *BioResources*, vol. 5, no. 4, 01 2010, pp. 2184–2194.

Lu, M., et al. "TiO_2-Modified Pd/SiO_2 for Catalytic Hydrodeoxygenation of Guaiacol," *Energy Fuels*, vol. 30, no. 8, Aug. 2016, pp. 6671–6676.

Luo, Y. R., "Comprehensive Handbook of Chemical Bond Energies." CRC press, 2007.

Luque, R. "Catalytic Chemical Processes for Biomass Conversion: Prospects for Future Biorefineries," *Pure and Applied Chemistry*, vol. 86, no. 5, 2014, pp. 843–857.

Lutz, W. "Zeolite Y: Synthesis, Modification, and Properties—A Case Revisited," *Advances in Materials Science and Engineering*, vol. 2014, 2014 pp. 1–20.

Martínez, C., et al. "Improved THETA-1 for Light Olefins Oligomerization to Diesel: Influence of Textural and Acidic Properties," *Topics in Catalysis,* vol. 57, no. 6–9, Apr. 2014, pp. 668–682.

Mitchell, S., et al. "Visualization of Hierarchically Structured Zeolite Bodies from Macro to Nano Length Scales," *Nature Chemistry*, vol. 4, no. 10, 01 2012, pp. 825–831.

Mohammed, I. Y., et al. "Comprehensive Characterization of Napier Grass as a Feedstock for Thermochemical Conversion," *Energies*, vol. 8, no. 5, May 2015, pp. 3403–3417.

Nimmanwudipong, T., et al. "Catalytic Reactions of Guaiacol: Reaction Network and Evidence of Oxygen Removal in Reactions with Hydrogen," *Catalysis Letters,* vol. 141, no. 6, Jun. 2011, pp. 779–783.

Olcese, R. N., et al. "Gas-Phase Hydrodeoxygenation of Guaiacol over Fe/SiO$_2$ Catalyst." *Applied Catalysis B*, vol. 115-116, 2012, pp. 63-73.

P. Mäki-Arvela and D. Y. Murzin, "Hydrodeoxygenation of Lignin-Derived Phenols: From Fundamental Studies towards Industrial Applications," *Catalysts,* vol. 7, no. 9, Sep. 2017, p. 265.

Pang, S. and A. S. Mujumdar, "Drying of Woody Biomass for Bioenergy: Drying Technologies and Optimization for an Integrated Bioenergy Plant," *Drying Technonolgy*, vol. 28, no. 5, May 2010, pp. 690–701.

Pérez-Ramírez, J. et al., "Expanding the Horizons of Hierarchical Zeolites: Beyond Laboratory Curiosity Towards Industrial Realization," *ChemCatChem*, vol. 3, no. 11, 01 2011, pp. 1731–1734.

Peters, J. E., et al. "Anisole and Guaiacol Hydrodeoxygenation Reaction Pathways over Selected Catalysts," *Energy Fuels*, vol. 29, no. 2, Feb. 2015, pp. 909–916.

Protásio, T. P., et al. "Brazilian Lignocellulosic Wastes for Bioenergy Production: Characterization and Comparison with Fossil Fuels," *BioResources,* vol. 8, no. 1, 01 2013, pp. 1166–1185.

Rahman, M. M, et al. "Preparation of Zeolite Y Using Local Raw Material Rice Husk as a Silica Source," *Journal of Scientific Research*, vol. 1, no. 2, Apr. 2009, pp. 285-291.

Roth, B., et al. "Are the Benefits of Yield Responses to Nitrogen Fertilizer Application in the Bioenergy Crop Miscanthus × giganteus Offset by Increased Soil Emissions of Nitrous Oxide?," *GCB Bioenergy*, vol. 7, no. 1, Jan. 2015, pp. 145–152.

Roussel, T., et al. "Hydrogen Storage Enhanced in Li-doped Carbon Replica of Zeolites: A Possible Route to Achieve Fuel Cell Demand," *Journal of Chemical Physics,* vol. 130, no. 17, May 2009, p. 174717.

Sachtler, W. M. H. and A. Y. u. Stakneev, "Electron-Deficient Palladium Clusters and Bifunctional Sites in Zeolites." *Catalysis Today*, vol. 12, issues 2-3, 1992, pp. 283-295.

Sang, S., et al. "Difference of ZSM-5 Zeolites Synthesized with Various Templates," *Catalysis Today,* vol. 93–95, Sep. 2004, pp. 729–734.

Shi, Y., et al. "Recent Progress on Upgrading of Bio-Oil to Hydrocarbons over Metal/Zeolite Bifunctional Catalysts." *Catalysis Science & Technology*, vol. 7, 2017, pp. 2385-2415.

Shin, H., et al. "Dealumination and Characterization of Chabazite for Catalytic Application," *Research of Chemical Intermediates*, vol. 37, no. 9, Nov. 2011, pp. 1239–1246.

Singh, S. K. and J. D. Ekhe, "Towards Effective Lignin Conversion: HZSM-5 Catalyzed One-Pot solvolytic depolymerization/Hydrodeoxygenation of Lignin into Value Added Compounds," *RSC Advances*, vol. 4, no. 53, 01 2014, pp. 27971–27978.

Sotelo-Boyas, R., and Y. Liu, T. Minowa, "Renewable Diesel Production from the Hydrotreating of Rapeseed Oil with Pt/Zeolite and NiMo/Al$_2$O$_3$ Catalysts." *Industrial & Engineering Chemistry Research,* vol. 50, issue 5, 2010, pp. 2791–2799.

Srivastava, R., et al. "Dealumination of Zeolite Beta Catalyst Under Controlled Conditions for Enhancing its Activity in Acylation and Esterification," *Catalysis Letters*, vol. 130, no. 3–4, May 2009, pp. 655–663.

Sukhbaatar, B., et al. "An Exploratory Study on the Removal of Acetic and Formic Acids from Bio-Oil," *BioResources*, vol. 4, no. 4, 01 2009, pp. 1319–1329.

Sun, J., et al. "Carbon-Supported Bimetallic Pd–Fe Catalysts for Vapor-Phase Hydrodeoxygenation of Guaiacol." *Journal of Catalysis,* vol. 306, 2013, pp. 47-57.

Talmadge, M. S., et al. "A Perspective on Oxygenated Species in the Refinery Integration of Pyrolysis Oil." *Green Chemistry*, vol. 16, 2014, pp. 407-453.

Tran, N. T. et al. "Hydrodeoxygenation of Guaiacol over Al-MCM-41 Supported Metal Catalysts: A Comparative Study of Co and Ni." *Procedia Engineering,* vol. 148, 2016, pp. 1252-1258.

Valle, B., et al. "Hydrothermally Stable HZSM-5 Zeolite Catalysts for the Transformation of Crude Bio-Oil into Hydrocarbons." *Applied Catalysis B: Environmental,* vol. 100, issues 1-2, 2010, pp. 318-327.

Velichkina, L. M. "Hydrogen-Free Domestic Technologies for Conversion of Low-Octane Gasoline Distillates on Zeolite Catalysts," *Theoretical Foundations of Chemical Engineering*, vol. 43, no. 4, Aug. 2009, pp. 486–493.

Wang, H., et al. "Recent Development in Chemical Depolymerization of Lignin: A Review," *Journal of Applied Chemistry,* vol. 2013, 2013, Jul. 2013, p. e838645.

Wang, L. et al. "Mesoporous ZSM-5 Zeolite-Supported Ru Nanoparticles as Highly Efficient Catalysts for Upgrading Phenolic Biomolecules," *ACS Catalysis*, vol. 5, no. 5, May 2015, pp. 2727–2734.

Wang, X. J. and C. L. Yan, "Synthesis of Nano-sized NaY Zeolite Composite from Metakaolin by Ionothermal Method with Microwave Assisted," *Inorganic Materials,* vol. 46, no. 5, May 2010, pp. 517–521.

Wang, Y. et al. "Hydrotreatment of Lignocellulosic Biomass Derived Oil using a Sulfided NiMo/γ-Al$_2$O$_3$ Catalyst." *Catalysis Science & Technology*, vol. 4, 2014, pp. 109-119.

Wang, Y., et al. "From Biomass to Advanced Bio-Fuel by Catalytic Pyrolysis/Hydro-Processing: Hydrodeoxygenation of Bio-Oil Derived from Biomass Catalytic Pyrolysis." *Bioresource Technology*, vol. 108, 2012, pp. 280-284.

Wang, Y., et al. "Hydrodeoxygenation of Bio-Oil over Pt-Based Supported Catalysts: Importance of Mesopores and Acidity of the Support to Compounds with Different Oxygen Contents." *RSC Advances*, vol. 3, 2013, pp. 12635-12640.

Wang, Y., et al. "Hydrodeoxygenation of Dibenzofuran over Noble Metal Supported on Mesoporous Zeolite." *Catalysis Communications*, vol. 12, issue 13, 2011, pp. 1201-1205.

Wang, Y., et al. "Synthesis of Hierarchical ZSM-5 Zeolites by Solid-State Crystallization and their Catalytic Properties." *Journal of Catalysis,* vol. 349, 2017, pp. 53-65.

Wang, Y., et al. "Zeolite with Trimodal Porosity by Desilication of Zeolite Nanocrystals Aggregate." *Journal of Solid-State Chemistry*, vol. 194, 2012, pp. 416-421.

Welker, C. M., et al. "Engineering Plant Biomass Lignin Content and Composition for Biofuels and Bioproducts," *Energies,* vol. 8, no. 8, Aug. 2015, pp. 7654–7676.

Xiang, M. et al., "Preparation of Mesoporous Zeolite ETS-10 Catalysts for High-Yield Synthesis of α,β-Epoxy Ketones," *ChemCatChem,* vol. 7, no. 3, Feb. 2015, pp. 521–525.

Zhang, H., et al. "Organic Structure Directing Agent-Free and Seed-Induced Synthesis of Enriched Intracrystal Mesoporous ZSM-5 Zeolite for Shape-Selective Reaction," *ChemCatChem*, vol. 5, no. 10, Oct. 2013, pp. 2874–2878.

Zhao, C. and J. Lercher, "Selective Hydrodeoxygenation of Lignin-Derived Phenolic Monomers and Dimers to Cycloalkanes on Pd/C and HZSM-5 Catalysts." *ChemCatChem,* vol. 4, issue 1, 2012, pp. 64-68.

Zhao, H. Y., et al. "Hydrodeoxygenation of Guaiacol as Model Compound for Pyrolysis Oil on Transition Metal Phosphide Hydroprocessing Catalysts." *Applied Catalysis A,* vol. 391, issues 1-2, 2011, pp. 305-310.

Zhao, Liang, et al. "Effects of Concentration on the Alkali-Treatment of ZSM-5 Zeolite: a Study on Dividing Points," *Journal of Materials Science*, vol. 45, no. 19, Oct. 2010, pp. 5406–5411.

Zhen, S., et al. "Zn+ Cations, Probable $T_{14}Zn_{12}$ and T_{16} Clusters, and Zeolite Desilication (Less Likely Dealumination): Crystallographic Study of the Incomplete Reaction of Zn Vapor with Tl+-Exchanged Zeolite X," *Journal of Physical Chemistry B*, vol. 104, no. 3, 2000, pp. 515–525.

Zhou, M., et al. "Water-Assisted Selective Hydrodeoxygenation of Guaiacol to Cyclohexanol over Supported Ni and Co Bimetallic Catalysts," *ACS Sustainable Chemistry and Engineering*, vol. 5, no. 10, Oct. 2017, pp. 8824–8835.

Zhu, X., et al. "Bifunctional Transalkylation and Hydrodeoxygenation of Anisole over a Pt/HBeta Catalyst." *Journal of Catalysis*, vol. 281, issue 1, 2011, pp. 21-29.